Construction and Building Materials 247 (2020) 118518

Contents lists available at ScienceDirect

Construction and Building Materials

journal homepage: www.elsevier.com/locate/conbuildmat

Evaluating prestress losses in a prestressed concrete girder railway bridge using distributed and discrete fibre optic sensors

Cong Ye [a,*], Liam J. Butler [b], Mohammed Z.E.B. Elshafie [c], Campbell R. Middleton [a]

[a] Department of Engineering, University of Cambridge, Trumpington Street, Cambridge CB2 1PZ, UK
[b] Lassonde School of Engineering, Bergeron Centre for Engineering Excellence, 11 Arboretum Lane, York University, Toronto, ON M3J 1P3, Canada
[c] Department of Civil and Architectural Engineering, College of Engineering, Qatar University, Qatar

HIGHLIGHTS

- Distributed and discrete fibre optic sensors were installed in prestressed beams.
- Strain data were recorded during beam manufacturing and for the first 2.5 years.
- Measured prestress losses were compared with code predictions (Eurocode and AASHTO).
- Both simplified and time-step methods were used for prestress loss predictions.

ARTICLE INFO

Article history:
Received 5 September 2019
Received in revised form 17 February 2020
Accepted 19 February 2020
Available online 3 March 2020

Keywords:
Fibre optic sensing
Prestressed concrete
Railway bridges
Structural health monitoring

ABSTRACT

This paper evaluates the data collected during a comprehensive monitoring campaign aimed at capturing the prestress loss behaviour of four 11.9 m prestressed concrete beams. These beams formed part of the superstructure of a newly-constructed railway bridge in Staffordshire, U.K. Two types of prestressed concrete beams were monitored, two TY7 internal beams and two TYE7 edge beams. Both distributed and discrete fibre optic sensor (FOS) systems were used to measure strain and temperature for the first two and a half years since the beams were cast. Prestress loss mechanisms were investigated in detail including immediate prestress losses due to elastic shortening of concrete and time-dependent prestress losses due to steel relaxation, concrete shrinkage and creep. Prestress loss predictions were calculated using both European and American standards, which were then compared with measured prestress losses. Both simplified and advanced time-step methods were used to provide more refined loss predictions by taking into account the interrelationships between various prestress loss mechanisms and the total prestress force at the time of interest. To provide better interpretation of the monitoring measurements, a sensitivity analysis was performed to evaluate the effects of various input parameter uncertainties on prestress loss predictions. It was found that (i) time-step methods produced prestress loss estimates that were lower compared with the simplified method; and (ii) code estimates of prestress losses using measured material properties gave reasonable agreement with the field measurements. As structurally-integrated FOS systems are becoming more commonplace and hold great potential, it is envisaged that they enable better understanding of field performance and thus facilitate data-informed asset management.

© 2020 Elsevier Ltd. All rights reserved.

1. Introduction

Prestressed concrete bridges comprise a significant proportion of the bridge stock both in the United Kingdom and around the world. The U.K.'s rail sector alone has more than 25,000 bridges and around one tenth of them are prestressed concrete bridges (pre-tensioned or post-tensioned), according to an internal report by the national rail provider, Network Rail [1]. Recent developments in construction technologies have increased the industry's familiarity with and confidence in adopting prestressed concrete structures (especially post-tensioned structures), and have led to a growing realisation of the benefits associated with these structures (e.g. generally more economical, higher material efficiency, reduced labour, quicker construction, etc.) [2]. As such, it is envisaged that prestressed concrete bridges may become an increasingly popular option for transport infrastructure in the near future. Therefore, it is essential that prestressed concrete bridges

* Corresponding author.
E-mail address: cy273@cam.ac.uk (C. Ye).

https://doi.org/10.1016/j.conbuildmat.2020.118518
0950-0618/© 2020 Elsevier Ltd. All rights reserved.

are managed and maintained properly to ensure the safety and serviceability of these infrastructure assets in the future.

A critical indicator of the structural performance of prestressed concrete bridge elements is their remaining level of prestress. This governs both the remaining load capacity (i.e. safety) and the in-service deflections (i.e. serviceability) of prestressed concrete bridges. The magnitude of the prestressing force decreases gradually throughout the life of a prestressed concrete structure. Both the magnitude and the rate of prestress loss are affected by many interdependent factors such as time-dependent material properties (e.g. concrete modulus of elasticity, concrete strength), material behaviour (e.g. concrete shrinkage and creep, steel relaxation) and structural conditions (e.g. reinforcement type, anchorage conditions, etc.). Current practice for evaluation of existing prestressed concrete bridges involves mostly visual inspection of concrete and steel conditions and sometimes the use of acoustic emission (AE) sensors for detecting wire breaks (e.g. [3,4]). Visual assessment poses issues of subjectivity, unreliability, late detection of damage and difficulty of relating observed damage to actual structural capacity [5,6], while AE sensors can produce data containing false positives and have an inherent difficulty in assessing the absolute condition of damage rather than its rate of change [3]. Therefore, an accurate understanding of short-term and long-term performance of prestress losses would be beneficial for improving decision making in asset management of these bridge structures.

Design equations for predicting prestress losses have primarily been derived and developed based on empirical results. A variety of structural design codes and technical documents from around the world include formulations for estimating the short- and long-term prestress losses. They include Eurocode 2, AASHTO (American Association of State Highway and Transportation Officials), PCI (Prestressed Concrete Institute), CEB-FIP 90 (The International Federation for Structural Concrete), ACI 2019 (American Concrete Institute), etc. [7–10]. Design guidance documents have also been published, such as [11–13]. However, there have been very few field studies which have measured prestress losses in real world prestressed concrete bridges (i.e. during their construction or in operation). Consequently, the nature of the progression of prestress losses in real world bridge applications is largely unknown and any resulting data comparing actual losses versus code predictions has rarely been available.

Recent developments in fibre optic sensing (FOS) technology for civil engineering structural health monitoring (SHM) applications have provided a unique opportunity for measuring the real behaviour of bridge structures and thus informing bridge operation and maintenance (O&M) decisions. This includes both discrete FOS such as Fibre Bragg gratings (FBGs) and distributed FOS such as Brillouin scattering-based techniques (e.g., Brillouin Optical Time Domain Reflectometry (BOTDR) and Brillouin Optical Time Domain Analysis (BOTDA)) and Rayleigh scattering-based techniques for measuring strain and temperature. FBGs can measure dynamic strain at specified point locations, while BOTDR and BOTDA can measure static strain along the entire length of a fibre optic cable. Temperature measurements can be used to compensate for the effects of temperature on FOS sensors (i.e. thermally imposed optical effects) and to decouple the effect of temperature-induced strain response from other effects (e.g. operational loadings, structural damage, etc.) acting on the bridge structures.

Middleton et al. [14] noted the often limited consideration of how the SHM data would be interpreted to extract useful information and inform decision making before installation of bridge SHM systems. The use of bridge SHM data for delivering real value to bridge whole-life management, particularly O&M, was recently examined by [3,14–16]. Five categories of SHM system deployments were proposed based on a comprehensive literature review of current bridge monitoring practice [15]. These categories include: (i) sensor deployment studies, (ii) anomaly detection, (iii) threshold check, (iv) model validation, and (v) damage detection. As for the present study, measured prestress losses are compared with predicted prestress losses using code equations and provisions, which is considered a form of model validation.

Deriving methods for systematically relating bridge SHM data to prior physics-based models (e.g. first principles, code equations and provisions, finite element models, etc.), by interpreting and explaining the discrepancies between sensor measurements and model predictions, has remained a key challenge in the research community. There have been numerous attempts of model updating, sometimes also referred to as structural or system identification, for bridge applications over the past two to three decades (e.g. [17–20]). These approaches aim to minimise the discrepancy between model predictions and sensor measurements by optimising model parameters and the modelling approach, either manually or automatically. As for FOS data interpretation, Bentz and Hoult [21] presented a case study of bridge model updating using distributed strain data based on engineering interpretation of the sensor data.

In the case of prestress losses, several studies have been conducted for interpreting measured prestress losses of prestressed concrete girders by relating sensor measurements to physics-based models. Webb et al. [22] performed direct comparison of strain measurements from fibre optic sensors along the prestressing strands and predictions from two different empirical prediction models considering creep and shrinkage (based on Eurocode 2 and research from Collins and Mitchell [23]). They found a good agreement between the predictions and the measurements; and the discrepancies were smaller in magnitude than the uncertainty of sensor measurements. Abdel-Jaber and Glisic [24] presented a systematic approach for uncertainty analysis of code predictions and sensor measurements to enable more rigorous comparison between FOS measured and code predicted prestress losses. They found that although code predictions and sensor measurements agreed reasonably well, code predictions were not necessarily overly conservative as often perceived. Huang et al. [25] presented a finite element model updating approach, informed by parametric studies and engineering judgement, for comparison with measured vertical deflections and observed crack patterns of a prestressed concrete bridge. Using the updated FE model predictions, they were able to estimate the realistic creep and shrinkage levels and prestress losses. Sousa et al. [26] performed parameter identification by best fitting EC2 models with real strain measurements and performed load tests to validate and update the FE model of the prestressed concrete bridge.

Overall, two research gaps have been identified by the authors, including (i) a lack of rigorous and systematic engineering interpretation of the discrepancies between measured and predicted prestress losses, informed by parametric studies; and (ii) the need for developing methods for better extracting useful information from prestress loss monitoring data to inform future bridge design and O&M practice.

This study serves as the culmination of a previous study Butler et al. [27] on early-age behaviour of four prestressed concrete beams prior to concrete deck casting for a newly constructed concrete railway bridge in Staffordshire, UK. Both discrete and distributed FOS arrays (i.e. FBG and BOTDR) were employed to monitor the early-age concrete behaviour. The four monitored beams were two TY7 internal beams (BM2 and BM3) and two TYE7 edge beams (BM1 and BM9), as shown in Fig. 1. The key monitoring stages are described in Table 1.

The previous study [27] focused on evaluating prestress losses for the first six months since concrete beam casting in the manu-

(a)

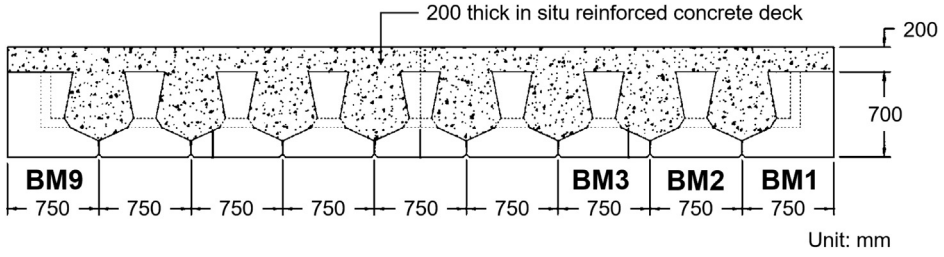

(b)

Fig. 1. (a) Underbridge 11 (Images by LJ Butler) and (b) cross-section of UB11 deck-girder system.

Table 1
Summary of the various stages of beam monitoring.

Stage	Description	Date(s)				Effects
		TY7 beams (BM2 and BM3)		TYE7 beams (BM1 and BM9)		
		Date	No. days after casting	Date	No. days after casting	
1	Baseline following beam casting	22 Jan 2015	0	9 Jan 2015	0	None prior to concrete initial set
2	Initial curing prior to transfer of prestress	22–29 Jan 2015	0–7	9–13 Jan 2015	0–4	Initial curing and steel relaxation
3	Pre- and post- transfer of prestress	29 Jan 2015	7	13 Jan 2015	4	Elastic shortening of concrete
3A*	Second stage casting, on TYE7 beams only	N/A	N/A	5 Mar 2015	55	Added dead load; creep; differential shrinkage
4	Outdoor storage in precast facility (early age curing, ~3 months)	14 Apr 2015	82	14 Apr 2015	95	Early age steel relaxation, shrinkage and creep
5	Prior to casting of bridge deck (after installation of reinforcing steel and transport of beams)	6 Jul 2015	165	6 Jul 2015	178	Transportation to site and continued steel relaxation, shrinkage and creep
6**	Pre- and post- deck casting	13 Jul 2015	172	13 Jul 2015	185	Added dead load; creep; differential shrinkage
7	Following deck curing	21 Jul 2015	180	21 Jul 2015	193	Continued steel relaxation, shrinkage and creep
8	Temporary haul road construction	28 Nov 2015	279	28 Nov 2015	292	Added live load; continued steel relaxation, shrinkage and creep
9	Prior to service	14 Mar 2016	417	14 Mar 2016	430	Continued steel relaxation, shrinkage and creep
10	4 months in-service	14 Jul 2016	539	14 Jul 2016	552	Continued steel relaxation, shrinkage and creep
11	1 year and 4 months in-service	7 Jul 2017	897	7 Jul 2017	910	Continued steel relaxation, shrinkage and creep

* Note: monitoring data was not recorded at the time of this event. Occurred on TYE7 beams only.
** Note: all beams were transported to site and were installed on the bridge abutments on 30 Jun 2015. Data was not recorded until one week later on 6 Jul 2015.

facturing facility, up until one week prior to the in-situ casting of concrete deck onto the concrete beams which had been installed onto the bridge abutments. This paper focuses on the time-dependent prestress loss behaviour up until approximately two and a half years since the concrete beams were cast. During the last one year and four months of this time duration, the beams had been in-service carrying live train loads. Time-dependent prestress losses as a result of continued concrete shrinkage, concrete creep and steel relaxation, as well as their interrelationships during different construction stages and in bridge operation, were evaluated.

This study undertakes a rigorous sensitivity analysis to aid in the evaluation and interpretation of prestress loss monitoring data. The results of this study can help improve the understanding of prestress loss behaviour of real world prestressed concrete bridges

both under construction and during operation. These monitoring results and their interpretation can also help establish a performance baseline for future structural health monitoring and data interpretation leading to data-informed performance-based asset management.

2. Monitoring system and programme

Underbridge 11 (UB11) is an 11.9 m prestressed concrete bridge with a cast-in-place concrete slab simply-supported on bearing type supports, as shown in Fig. 1. It is located along the West Coast Main Line in Staffordshire, U.K., and carries a single lane of railway. The four monitored beams were fabricated in January 2015 at Laing O'Rourke's Explore Industrial Park (EIP) manufacturing facility in Worksop, UK. They were then transported to and installed on site as bridge girders which form part of the UB11. Two of the four monitored beams are TYE7 edge beams (BM1 and BM9) and the other two are TY7 internal beams (BM2 and BM3).

Fig. 2 shows the cross-sectional dimensions of the monitored beams and the sensor layout, both FBG and BOTDR, for both types of beams. These sensors were installed during the manufacturing of the beams. Both strain FBGs and temperature compensating FBGs were used to measure the mechanical strain and compensate for the effects of temperature. The strain measuring FBGs can measure strain changes within ±5με and there were 20 FBGs per sensor array spaced at one metre centre to centre. The temperature measuring FBGs have a temperature accuracy of ±1.0 °C and were comprised of 6 FBGs per sensor array. The BOTDR cables were capable of measuring static distributed strain within ±50 με. The temperature measuring BOTDR has a temperature accuracy of ±1.0 °C. Cable coatings for both FBG and BOTDR sensors were carefully selected to ensure long-term sensor accuracy, robustness and durability. Further details of the sensor specifications, installation and data collection are provided in Butler et al. [27].

For FBG sensors, the calculation of mechanical strain (considering temperature compensation) can be performed using Eq. (1).

$$\varepsilon_m = \frac{1}{k}\left(\frac{\Delta\lambda_m}{\Delta\lambda_{om}} - \frac{\Delta\lambda_c}{\Delta\lambda_{oc}}\right) \quad (1)$$

where

$\Delta\lambda_m$ = wavelength shift of strain-measuring FBG
$\Delta\lambda_{om}$ = base wavelength of strain-measuring FBG
$\Delta\lambda_c$ = wavelength shift of temperature compensation FBG
$\Delta\lambda_{oc}$ = base wavelength of temperature compensation FBG

For BOTDR, the mechanically induced strain from Brillouin frequency shift can be calculated using Eq. (2).

$$\upsilon_b(s) = \upsilon_{bo} + M\varepsilon(s) \quad (2)$$

where

$\nu_b(s)$ = Brillouin frequency shift as a function of distance
ν_{bo} = Brillouin frequency shift with zero induced strain
M = a constant of proportionality
$\varepsilon(s)$ = thermally/mechanically induced strain as a function of distance

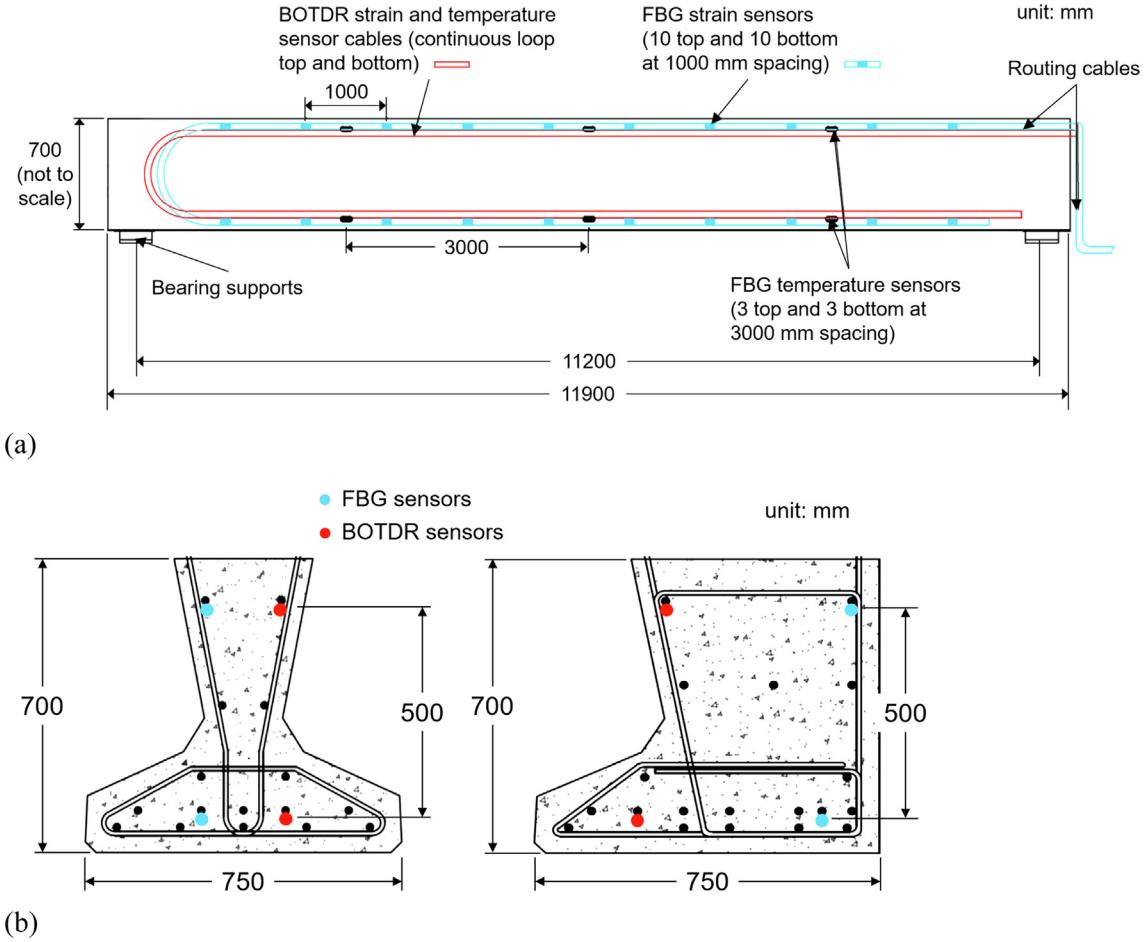

Fig. 2. (a) Typical fibre optic sensor layout and (b) prestressed concrete beam cross sections – edge TYE7 beams (left) and internal TY7 beams (right).

The various stages of beam monitoring are summarised in Table 1. Note that BM1 and BM2 do not have data collected on stage 5 for July 6, 2015, and BM3 and BM9 do not have data collected on stages 6 and 7 for July 13 and 21, 2015, respectively.

3. Prestress loss predictions

3.1. Prestress loss development of precast prestressed concrete beams

By considering the change in prestressing force, changes in material properties and changes in section geometry over time, the strains at various locations along the beams and along the cross-section depth can be calculated using Eq. (3).

$$\varepsilon(x,y,t) = \frac{P(x,t)}{A_c(t)E_c(t)} + \frac{[M_{sw}(x,t)+M_{qp}(x,t)+P(x,t)e(t)]y}{E_c(t)I_c(t)} \quad (3)$$

where P is the total prestress force in tendons; M_{sw} is the bending moment due to self-weight; M_{qp} is the bending moment due to quasi-permanent service load; e is the eccentricity of the centroid of all tendons relative to the centroid of the (uncracked) cross section; x is the distance measured along the length of the beam, and y is the distance measured from the top of the beam cross-section to its geometric centroid.

In addition to instantaneous prestress losses due to anchorage set, friction and elastic shortening (friction loss primarily occurs in post-tensioned construction), the prestressing force will also change with time as various time-dependent material-related mechanisms such as steel tendon relaxation, concrete shrinkage and concrete creep evolve. In conjunction, the various stages of construction and their associated quasi-permanent loading (refer to Table 1) all influence the change in total prestress force in the prestressing tendons. To capture the evolution of this changing force, a time-step method can be used to calculate sequential changes in prestress force as described by Hendy and Smith [11] for use with the Eurocode 2 and by Naaman [13] for use with the AASHTO-LRFD model code. As the level of prestress in steel tendons and various prestress loss mechanisms (i.e. steel relaxation, concrete shrinkage and concrete creep) are interrelated, incremental prestress losses for these mechanisms as well as the remaining prestress force needs to be re-calculated at each time step (e.g. at each day, or between successive construction stages). Furthermore, it may be significant to account for the effects of differential shrinkage and creep strains that arise from casting of the concrete deck after the prestressed concrete beams have undergone some initial levels of relaxation, creep and shrinkage.

The accuracy of prestress loss predictions depends not only on the accuracy of code equations and provisions, but also on the accuracy of key input parameters. These parameters include material properties, section geometry, boundary conditions, applied loadings, environmental conditions, etc. Based on the bridge designer's calculations, the initial prestress force was assumed to be 209 kN for each prestressing tendon (corresponding to 1393 MPa). These initial prestressing levels were later confirmed by the prestressing facility operator's calculations. All of the prestressed concrete beams were cast using self-compacting concrete (SCC) of strength class C60/75. The material and section geometry properties of the beams are summarised in Table 2.

Prestress losses are complex to accurately estimate, as they are influenced by a number of factors, which include (i) time to transfer of prestressing force (i.e. detensioning) since concrete beam casting, (ii) age of girders at the time of deck casting, (iii) type of prestressing strands, (iv) concrete material properties (e.g. compressive strength, modulus of elasticity), (v) initial stresses in concrete (e.g. due to prestress), and (vi) storage conditions (e.g. ambient relative humidity, temperature and the amount of air exposure), etc. In general, (i) affects the concrete properties at the time of transfer and thus the amount of elastic shortening; (ii) affects the amount of differential creep and shrinkage; (iii) affects steel properties (e.g. relaxation properties, maximum allowable prestress force, etc.), which in turn affect various prestress loss mechanisms, e.g. low relaxation steel has lower relaxation steel compared with stress relieved loss; (iv) affects elastic shortening, concrete creep and concrete shrinkage; (v) affects creep loss; and (vi) affects various prestress loss mechanisms, particularly shrinkage loss. A sensitivity analysis is performed in a later section to quantitatively examine the effect of each factor (in particular, key input parameters to the code formulae) and thus determine their relative importance to prestress loss predictions.

Table 2
Material and geometry properties of prestressed concrete beams.

Material or section geometry property	TY7 beams	TYE7 beams
Casting date	22 Jan 2015	9 Jan 2015
Concrete material properties		
Water/cementitious materials ratio	0.36	0.36
Slump flow	760 mm	770 mm
Design $f_{ck,cube}$ (28 days)	75 MPa	75 MPa
$f_{ck,cube}$ (28 days)[1]	89.6 MPa	90.7 MPa
$f_{ck,cube}$ (7 days)[1]	75.8 MPa	76.7 MPa
$f_{ck,cube}$ at transfer[2]	60.5 MPa	65.8 MPa
Estimated E_{cm} at transfer[3]	35,300 MPa	36,210 MPa
Steel material properties		
Prestressing steel (7 wire strand)[4]	16 strands	19 strands
f_{pu}	1860 MPa	1860 MPa
E_p	195,000 MPa	195,000 MPa
ρ_{1000} (elongation after 1000 h)	2.5%	2.5%
Section geometry		
A_{strand}	150 mm^2	150 mm^2
Beam length, L[4]	11.9 m	11.9 m
Area of uncracked gross section, A_c[5]	272194 mm^2	398330 mm^2
Moment of inertia of uncracked gross section, I_c[5]	1.26×10^{10} mm^2	1.75×10^{10} mm^2
Eccentricity of tendons in uncracked gross section, e_{cp}[5]	80.9 mm	125 mm

[1] Measured values are based on cube specimens cured under controlled conditions, i.e. in water bath.
[2] Estimate based on measured maturity versus temperature data provided by contractor (detensioning of TYE7 beams occurred 94 h after casting).
[3] $E_{cm}(1) = (f_{cm}(1)/f_{cm}(28))^{0.3}E_{cm}(28)$; $E_{cm}(28) = 22(f_{cm}(28)/10)^{0.3}$; $f_{ck}(t) = 0.8f_{ck,cube}(t)$.
[4] Based on supplier specification sheets.
[5] Based on designers' calculation sheets. Value relative to centroid of the beam cross section (below the centroid).

To provide a basis for comparing prestress losses which have been calculated from measured fibre optic strain data, prestress losses were predicted using three different methods with different levels of model fidelity. Two of the methods are based on Eurocode 2 [7] and Hendy and Smith [11]: one simplified method and one time-step method (with time-steps of one day). The third method is based on AASHTO-LRFD [8] and Naaman [13], which is a time-step method specifically tailored for segmental construction of prestressed concrete girder bridges (with time-steps corresponding to different construction stages).

3.2. Overview of prestress loss calculations

3.2.1. EC2 simplified method

This section describes in detail a simplified method based on Eurocode 2. For this case study, due to the detensioning procedures adopted at the precasting facility, it was assumed any immediate losses due to anchorage set were negligible.

Table 3 presents a summary of Eurocode 2 equations for estimating prestress losses. In this study, prestress losses in the prestressed concrete beams were evaluated at a series of monitoring

Table 3
Summary of Eurocode 2 formulae for prestress loss predictions.

Prestress loss mechanism	Eurocode 2 formulae
Relaxation of tendons	$\Delta P_{REL,i} = 6.6A_p(\sigma_{pi})\rho_{1000}e^{9.1\mu}\left(\frac{t}{1000}\right)^{0.75(1-\mu)} \times 10^{-6}$ where $\mu = \frac{\sigma_{pi}}{f_{pk}}$
Elastic shortening of concrete	$\Delta P_{ES}(t) = \frac{A_p\frac{E_p}{E_{cm}(t)}\sigma_c}{1+\frac{E_p}{E_{cm}(x)}\frac{A_p}{A_c}\left(1+\frac{A_c}{I_c}e_{cp}{}^2\right)}$ where $\sigma_c = \frac{P}{A_g} + \frac{(M_{sw}+M_{qp}+Pe)e}{I_g}$
Combined time-dependent creep, shrinkage and steel relaxation	$\Delta P(t)_{C+S+R} = A_p\Delta\sigma_{p,c+s+r} = A_p\frac{\varepsilon_{cs}E_p+0.8\Delta\sigma_{pr}+\frac{E_p}{E_{cm}}\varphi(t,t_0)\sigma_{c,qp}}{1+\frac{E_p}{E_{cm}}\frac{A_p}{A_c}\left(1+\frac{A_c}{I_c}e_{cp}^2\right)[1+0.8\varphi(t,t_0)]}$
Autogenous shrinkage of concrete	$\varepsilon_{ca}(t) = \beta_{as}(t)\varepsilon_{ca}(\infty)$ where $\varepsilon_{ca}(\infty) = 2.5(f_{ck}-10)\times10^{-6}$ and $\beta_{as}(t) = 1-e^{-0.2t^{0.5}}$
Drying shrinkage of concrete	$\varepsilon_{cd}(t) = \beta_{ds}(t,t_s)k_h\varepsilon_{cd,0}$ where $\beta_{ds}(t,t_s) = \frac{t-t_s}{(t-t_s)+0.04\sqrt{h_0{}^3}}$ and $\varepsilon_{cd,0} = 0.85\left[(220+110\alpha_{ds1})e^{\left(-\alpha_{ds1}\frac{f_{cm}}{10}\right)}\right]\beta_{RH}\times10^{-6}$ and k_h is a function of h_0 (using a lookup table)
Concrete creep	$\varepsilon_\infty = \frac{\sigma_c}{E_{c,eff}}$ where $E_{c,eff} = \frac{E_c}{\varphi(t,t_0)}$ and $\varphi(t,t_0) = \varphi_0\beta_c(t,t_0)$
Total prestress losses	$\Delta P_{TOT} = \Delta P_{ES} + \Delta P_{C+S+R}$ and %Loss = $\Delta P_{TOT}/\Delta P_i$

* Key notations:
E_c = tangent modulus of elasticity of concrete.
h_0 = notional size of cross-section ($h_0 = 2A_c/u$).
u = length of perimeter exposed to drying.
β_{as} = age of concrete factor for autogenous shrinkage strain.
$\beta_c(t, t_0)$ = a coefficient used to describe the development of creep with time after loading.
β_{ds} = age of concrete factor for drying shrinkage strain.
β_{RH} = relative humidity factor.
ΔP_{C+S+R} = absolute value of the variation of force in tendons due to creep, shrinkage and relaxation at location ×, at time t.
$\Delta\sigma_{pr}$ = absolute value of the variation in stress in tendons at location x, at time t, due to the relaxation of the prestressing steel.
ε_{cs} = total shrinkage strain (autogenous + drying) = $\varepsilon_{ca} + \varepsilon_{cd}$.
ε_∞ = final creep strain.
σ_c = elastic stress in concrete.
$\sigma_{c,qp}$ = stress in the concrete adjacent to tendons at time t, due to self-weight, initial prestress and other quasi-permanent actions.
σ_{pi} = stress in the tendons after immediate losses.
ρ_{1000} = relaxation loss 1000 h after tensioning at 20 °C.
φ_0 = notional creep coefficient.
$\varphi(t,t_0)$ = creep coefficient at time t for a load application occurring at time t_0.

and construction stages, as previously shown in Table 1. Losses due to steel relaxation, elastic shortening of concrete, concrete shrinkage and concrete creep were considered. Monitoring data from both the FBG and BOTDR sensors were recorded at all stages of prestress loss for the two edge beams (BM1 and BM9) and the two internal beams (BM2 and BM3). Prestress loss estimates based on calculations suggested by the Eurocode 2 were then compared with the measured prestress losses.

3.2.2. EC2 time-step method

This section describes an iterative time-step method (Hendy and Smith [12] and Naaman [14]) based on Eurocode 2 in order to provide a more accurate comparison between the predicted and measured prestress losses. The time-step method accounts for the interrelationships between various time-dependent prestress loss mechanisms, the evolution of concrete material properties and the change of total prestress force over time. A series of iterative calculations were performed between (i) level of total prestress in tendons at every time step; (ii) relevant input parameters to update (e.g. material properties, section geometry, loadings, etc.) at every time step; and (iii) incremental prestress losses of the time-dependent prestress loss mechanisms at every time step. Concrete properties, particularly compressive strength and modulus of elasticity evolve over time as a result of curing and continued hydration. Applied loading and internal stress distribution change over time as a result of segmental construction and continued change of total prestress force. For example, the casting of the concrete deck over the supporting prestressed concrete girders resulted in differential creep as a result of increased dead load and induced stress redistribution which was due to the deck-girder composite action. In this study, a time-step of one day (i.e. 24 h) was chosen for the EC2 time-step method to provide a more detailed estimate of prestress losses in the girders.

It is expected that the time-step method would give a lower prestress loss prediction compared with the basic method, particularly as a result of lower predictions of creep and relaxation losses. For relaxation loss, because the level of prestress in tendons is updated to account for continued prestress losses over time, the time-step method prediction would be lower due to the continuously updated 'initial' prestress force which decreases over time. For creep loss, because the prestress force is updated and decreases over time, the associated concrete stress and prestress loss due to creep are reduced. It has been found in this case study that reduction in creep loss prediction accounts for the majority of the reduction in total prestress loss prediction for the time-step method. The time-step method results in 2.9% and 1.7% reductions in the final prestress loss prediction (%) (i.e. the total design life prestress loss) for TY7 and TYE7 beams respectively, of which 1.8% and 1.3% are reductions in creep loss prediction for TY7 and TYE7 beams respectively.

3.2.3. AASHTO time-step method

The time-step method for estimating prestress losses in AASHTO-LRFD [8] is tailored for segmental construction of prestressed concrete girder bridges and takes into account two different stages: from concrete beam casting to deck placement and from deck placement up until the final design life. Table 4 presents a summary of the AASHTO-LRFD time-step method equations for estimating prestress losses. It should be noted that AASHTO-LRFD uses the U.S. customary units with basic units of feet (length), inches (length) and pounds (force). Therefore, the values of input parameters in SI units were first converted to the U.S. customary units to perform the calculations, and the final results (i.e. predictions of prestress losses) were then converted back to the SI units for further examination.

3.3. Assumptions and sources of error

A number of specific assumptions were implemented in this case study when using the above-noted methods. These assumptions may affect the prestress loss prediction and measurement and they are summarised as follows:

i. Prestressing tendons and the concrete were assumed to be perfectly bonded, and therefore any strain change in prestressing tendons was fully transferred to the surrounding concrete. It was also assumed that the FOS sensors were fully bonded to the surrounding concrete. This would mean that the FOS sensors attached to the prestressing strands were subjected to the same strain changes experienced by the prestressing tendons.
ii. Prestress losses due to anchorage set were assumed to be negligible due to the detensioning procedures adopted.
iii. The initial prestress force was assumed to be 209 kN per tendon (corresponding to 1393 MPa) based on both the designers' and the precast facility operator's calculations.
iv. Some material properties of concrete (e.g. 28-day and 7-day strengths) were measured, as shown in Table 2. For estimation of concrete strength evolution in the time-step meth-

Table 4
Summary of AASHTO-LRFD formulae for prestress loss predictions using the time-step method.

Prestress loss mechanism	AASHTO-LRFD formulae
Time of transfer to time of deck placement	
Shrinkage of girder concrete	$\Delta f_{pSR} = \varepsilon_{bid}\, E_p\, K_{id}$ where $K_{id} = \frac{1}{1+\frac{E_p A_{ps}}{E_{ci} A_g}\left(1+\frac{A_g e_{pg}^2}{I_g}\right)\left[1+0.7\psi_b(t_f,t_i)\right]}$
Creep of girder concrete	$\Delta f_{pCR} = \frac{E_p}{E_{ci}} f_{cgp}\psi_b(t_d,t_i)K_{id}$
Relaxation of prestressing strands	$\Delta f_{pR1} = \frac{f_{pt}}{K_L}\left(\frac{f_{pt}}{f_{py}} - 0.55\right)$ and may be assumed to equal to 1.2 ksi for low relaxation strands
Time of deck placement to final time	
Shrinkage of girder concrete	$\Delta f_{pSD} = \varepsilon_{bdf}\, E_p\, K_{df}$ where $K_{df} = \frac{1}{1+\frac{E_p A_{ps}}{E_{ci} A_c}\left(1+\frac{A_c e_{pc}^2}{I_c}\right)\left[1+0.7\psi_b(t_f,t_i)\right]}$
Creep of girder concrete	$\Delta f_{pCD} = \frac{E_p}{E_{ci}} f_{cgp}\left[\psi_b(t_f,t_i) - \psi_b(t_d,t_i)\right]K_{df} + \frac{E_p}{E_c}\Delta f_{cd}\psi_b(t_f,t_d)K_{df}$
Relaxation of prestressing strands	$\Delta f_{pR2} = \Delta f_{pR1}$
Shrinkage of deck concrete	$\Delta f_{pSS} = \frac{E_p}{E_c}\Delta f_{cdf} K_{df}\left[1+0.7\psi_b(t_f,t_d)\right]$ where $\Delta f_{cdf} = \frac{\varepsilon_{ddf} A_d E_{cd}}{\left[1+0.7\psi_d(t_f,t_d)\right]}\left(\frac{1}{A_c} - \frac{e_{pc} e_d}{I_c}\right)$
Total	
Total prestress losses	$\Delta f_{pLT} = \left(\Delta f_{pSR} + \Delta f_{pCR} + \Delta f_{pR1}\right)_{id} + \left(\Delta f_{pSD} + \Delta f_{pCD} + \Delta f_{pR2} - \Delta f_{pSS}\right)_{df}$ = prestress loss between transfer and deck placement + prestress loss after deck placement

* Key notations:
A_c = area of section calculated using the gross composite concrete section properties of the girder and the deck (in.^{2}).
A_d = area of deck concrete (in.^{2}).
E_{cd} = modulus of elasticity of deck concrete (ksi).
e_d = eccentricity of deck with respect to the gross composite section (in.).
e_{pc} = eccentricity of prestressing force with respect to centroid of composite section (in.).
e_{pg} = eccentricity of prestressing force with respect to centroid of girder (in.).
I_c = moment of inertia of section calculated using the gross composite concrete section properties of the girder and the deck (in.^{4}).
f_{pt} = stress in prestressing strands immediately after transfer, taken not less than $0.55f_{py}$.
K_L = 30 for low relaxation strands and 7 for other prestressing steel, unless more accurate manufacturer's data are available.
K_{id} = transformed section coefficient that accounts for time-dependent interaction between concrete and bonded steel in the section being considered for time period between transfer and deck placement.
K_{df} = transformed section coefficient that accounts for time-dependent interaction between concrete and bonded steel in the section being considered for time period between deck placement and final time.
t_d = age at deck placement (days).
t_f = final age (days).
t_i = age at transfer (days).
Δf_{cd} = change in concrete stress at centroid of prestressing strands due to long-term losses between transfer and deck placement, combined with deck weight and superimposed loads (ksi).
Δf_{cdf} = change in concrete stress at centroid of prestressing strands due to shrinkage of deck concrete (ksi).
ε_{bdf} = shrinkage strain of girder between time of deck placement and final time.
ε_{bid} = concrete shrinkage strain of girder between the time of transfer and deck placement.
ε_{ddf} = shrinkage strain of deck concrete between placement and final time.
ψ_b = girder creep coefficient.

ods, the 28-day strength value was used and the strength values at the other dates were derived based on EC2 formulae.

v. It was assumed that concrete cracking was negligible during the early-age of the prestressed concrete beams (e.g. first two years), and thus uncracked gross section properties were used throughout the calculations.

Overall, there are three main sources of errors which could account for the discrepancy between code predictions and sensor measurements: input parameter errors, code formulae errors and data/sensor errors. Input parameter errors include inaccurate assumptions and estimations of various input parameters to the code formulae, which include material properties, section geometry, applied loading, boundary condition, environmental conditions (e.g. temperature, humidity), etc. A sensitivity analysis is conducted in the next section to evaluate the effect of each parameter on the final prestress loss prediction. Code formulae errors are more difficult to specify and quantify as some of the errors or uncertainties are non-parametric, for example, mathematical form (e.g. polynomial, exponential, etc.) of each equation, key assumptions in the modelling process (e.g. which factors are significant and which ones can be neglected), etc. As for data errors, there are three types of measurement errors: (i) the validity of the measurement itself, i.e. data accuracy and precision; (ii) the validity of what is being measured, i.e. whether what is supposed to be measured is actually being measured; and (iii) the validity of indirect or alternative measurements. In this study, FBG strain measurements have a precision of ±5με and BOTDR strain measurements have a precision of ±50με. As for the second type of measurement error, if the FOS strain sensors were not properly bonded to the concrete surrounding the prestressing steels and temperature compensation was not properly conducted, the measured strain would not be the actual strain of interest.

3.4. Sensitivity analysis

3.4.1. Sensitivity analysis overview

To evaluate the effect of various assumptions on prestress loss predictions, particularly various input parameter values, a sensitivity analysis, along with a qualitative uncertainty analysis, was performed to evaluate the importance of each parameter to the final prestress loss prediction (i.e. the total design life prestress loss). These input parameters, as mentioned in the previous section, include material properties (e.g. strength, modulus of elasticity, mass density, etc.) of concrete and steel, section geometry (e.g. cross-sectional area, second moment of area, eccentricity of prestressing tendons, etc.), applied loading (e.g. self-weight, quasi-permanent load, prestress force, etc.), and environmental conditions (e.g. temperature, humidity, etc.).

To enable comparison of sensitivity across different parameters of different structural elements, a normalised measure of sensitivity based on Brownjohn et al. [17] was calculated as the ratio of percentage change of output response and percentage change of input parameter.

$$S_{i,j}^{N} = \frac{\partial R_i}{\partial P_j}\frac{P_j}{R_i} \approx \frac{\Delta R_i}{R_i} / \frac{\Delta P_j}{P_j} \tag{4}$$

The relationship between the input parameter of interest and the output prestress loss prediction may be nonlinear, and therefore a number of values within the reasonable range of each input parameter (e.g. original value, ±5%, ±10%, ±15%, ±20%) as well as the corresponding prestress loss predictions were used to investigate both the sensitivity and the linearity relationship in order to inform the evaluation of code predictions and monitoring results.

One caveat to note is that some of these input parameters are related, as given by the code equations, and their relationships can be different between EC2 and AASHTO-LRFD. For example, concrete modulus of elasticity is estimated from concrete compressive strength in both codes. However, in AASHTO-LRFD, concrete modulus of elasticity is also a function of concrete mass density which is a function of concrete compressive strength. Specifically, in EC2,

$$E_{cm}(t) = 22(f_{cm}(t)/10)^{0.3} \tag{5}$$

and in AASHTO-LRFD,

$$E_c = 33000 w_c^{1.5}\sqrt{f_c} \tag{6}$$

where w_c is concrete mass density and is estimated as $w_c = 0.14 + 0.001 f_{ci}$. Therefore, changing the value of one input parameter may also simultaneously change some other parameters, and care must be taken prior to interpreting the sensitivity analysis results.

Eleven key input parameters were examined: mass density of concrete, compressive strength of concrete, modulus of elasticity of concrete, tensile strength of steel, modulus of elasticity of steel, initial prestress force, applied loading (self-weight and quasi-permanent loading), relative humidity, cross-sectional area of the concrete beam, second moment of area of the concrete beam, and eccentricity of the prestressing tendons. Note that temperature is not a direct input parameter into the code equations, but it would affect concrete material properties which were examined in the sensitivity analysis. Thermal strains were not considered in the code predictions and were filtered out when processing the FBG and BOTDR data. The surface area of the concrete beam which is exposed to air can also affect the prestress loss prediction. However, after performing a sensitivity analysis, this effect was found to be very small and was not included in the following study.

3.4.2. Sensitivity analysis results: EC2 simplified and time-step methods

Figs. 3 and 4 present a summary of the sensitivity analysis results for the two EC2 methods (basic and time-step). It should be noted that in EC2, concrete modulus of elasticity is estimated from concrete compressive strength, and therefore a change in the concrete compressive strength would simultaneously change the estimation of concrete modulus of elasticity in the sensitivity analysis. To decouple these effects, a separate analysis with only changes in concrete modulus of elasticity was performed. It has also been found that most of these relationships between input parameter and output prediction are linear, except for the characteristic tensile strength of prestressing tendons and initial prestress force. This is due to the nonlinear relationship between relaxation loss prediction and these two input parameters, as shown in Table 3.

The accuracy of the time-dependent concrete material properties models may also have an effect on prestress loss prediction. As an example, in EC2, the evolution of concrete compressive strength is captured using

$$f_{cm}(t) = \beta_{cc}(t) f_{cm}(28) \tag{7}$$

where $\beta_{cc}(t) = \exp\{s[1 - (28/t)^{0.5}]\}$ with s being a coefficient which depends on cement type. The accuracy of this model (e.g. mathematical form of the equation, etc.) is a non-parametric uncertainty which is more difficult to examine and quantify. In this case study, it was assumed that the effect of this error would be much smaller than the effect of parameter error of concrete material properties, as the measurements of 28-day and 7-day concrete strengths were found to fit well with the EC2 predictive model of concrete strength evolution.

3.4.3. Sensitivity analysis for AASHTO method

Figs. 5 and 6 present a summary of the sensitivity analysis results for the AASHTO time-step method. It should be noted that in AASHTO-LRFD, concrete modulus of elasticity is estimated from concrete compressive strength and concrete mass density, and therefore changes in these two parameters would simultaneously change the estimation of concrete modulus of elasticity in the sensitivity analysis. In addition, concrete mass density is estimated from concrete compressive strength in AASHTO-LRFD, and therefore change of concrete compressive strength would also simultaneously change the estimation of concrete mass density in the sensitivity analysis. It has also been found that similar to the case in EC2, most of these relationships between input parameter and output prediction are linear, except for tensile strength of prestressing tendons and initial prestress force. This is accounted for by the assumptions in AASHTO-LRFD relaxation loss prediction that relaxation loss has a minimum value of 1.2 ksi for low-relaxation strands and stress in prestressing strands immediately after transfer is not less than $0.55 f_{py}$, as shown in Table 4.

3.4.4. Evaluation and interpretation of sensitivity analysis results

The sensitivity analysis revealed similar results for all three predictive models, with a few discrepancies. The effect of each input parameter on the overall predicted prestress loss are summarised as follows, based on Figs. 3–6:

i. Concrete material properties (mass density, γ_c, compressive strength, f_c, and modulus of elasticity, E_c): These parameters are interrelated in both codes. Varying γ_c alone has a negligible effect on prestress loss prediction. In EC2, γ_c is not explicitly used other than for estimating the self-weight of girders and deck (M_{sw}), which appears to have a small effect on prestress loss predictions (i.e. low sensitivity). Changing both f_c and E_c has a significant effect on prestress loss prediction, with changing E_c accounting for most of this effect.
ii. Steel material properties (characteristic tensile strength, f_{pk}, and modulus of elasticity, E_p): In EC2, the relationship between f_{pk} and prestress loss prediction is highly nonlinear, which is due to the nonlinear relationship between relaxation prediction ΔP_{CR} and f_{pk}. In AASHTO-LRFD, the relationship between f_{pk} and prestress loss prediction is also nonlinear, which is due to the code provision that relaxation loss has a minimum value of 1.2 ksi for low relaxation strands. Across all three methods, E_p was shown to have the greatest effect on prestress loss prediction compared to other parameters.

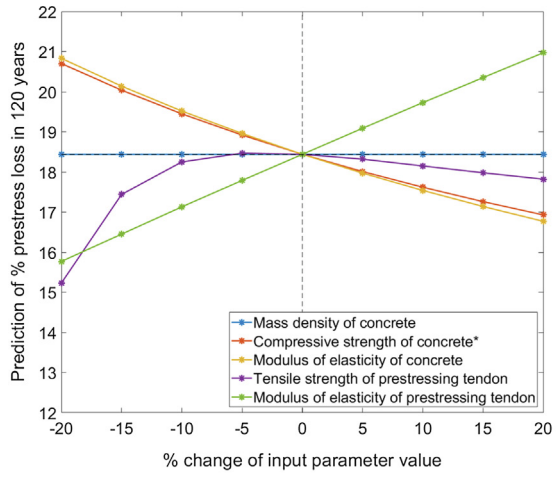

(a) EC2 basic – material

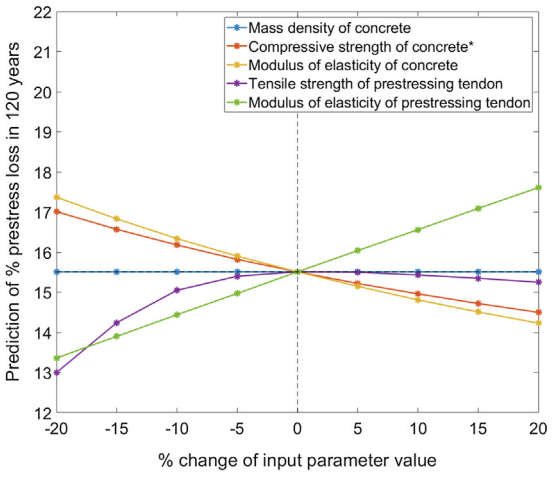

(b) EC2 time-step – material

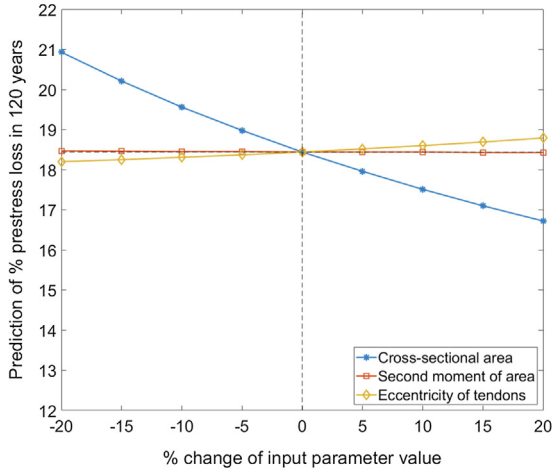

(c) EC2 basic – geometry

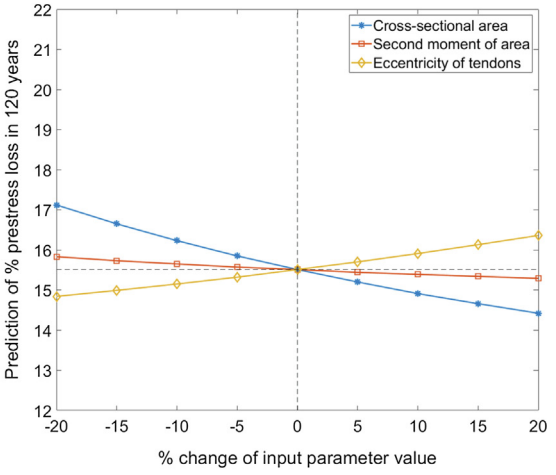

(d) EC2 time-step – geometry

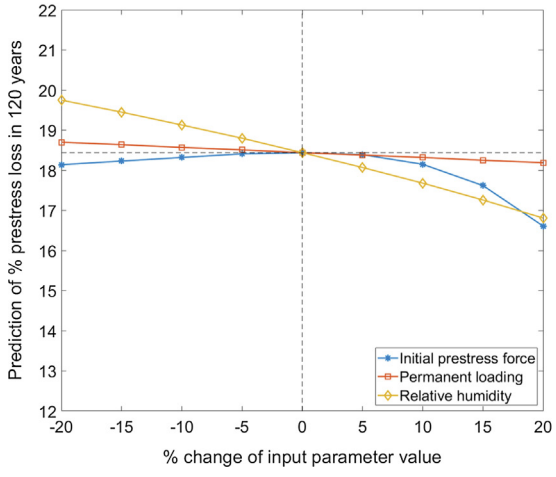

(e) EC2 basic – loading and environment

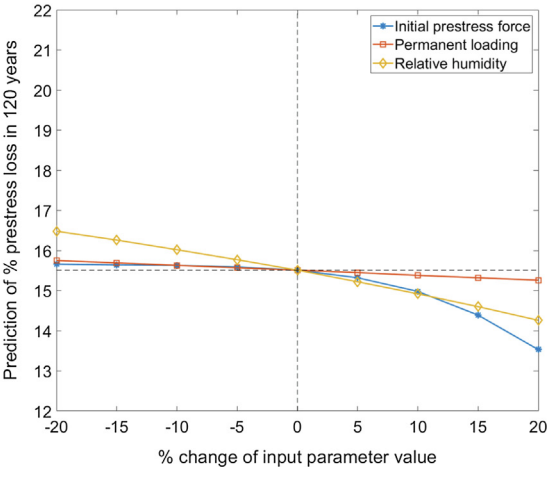

(f) EC2 time-step – loading and environment

Fig. 3. Sensitivity analysis results for EC2 methods.*Note: Change of compressive strength of concrete would simultaneously change the estimation of concrete modulus elasticity in EC2.

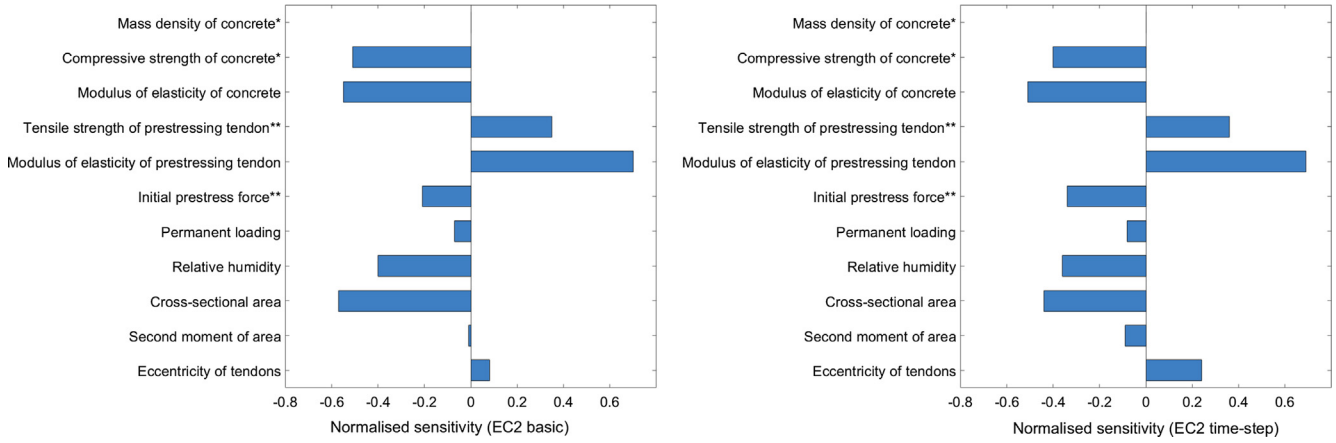

(a) EC2 basic (b) EC2 time-step

Fig. 4. Sensitivity analysis results for EC2 methods: normalised sensitivity.*Note: Mass density of concrete is not explicitly used for prestress loss prediction in EC2. Change of compressive strength of concrete would simultaneously change the estimation of concrete modulus elasticity in EC2.**Note: Relationship between input parameter and output prestress loss prediction is nonlinear.

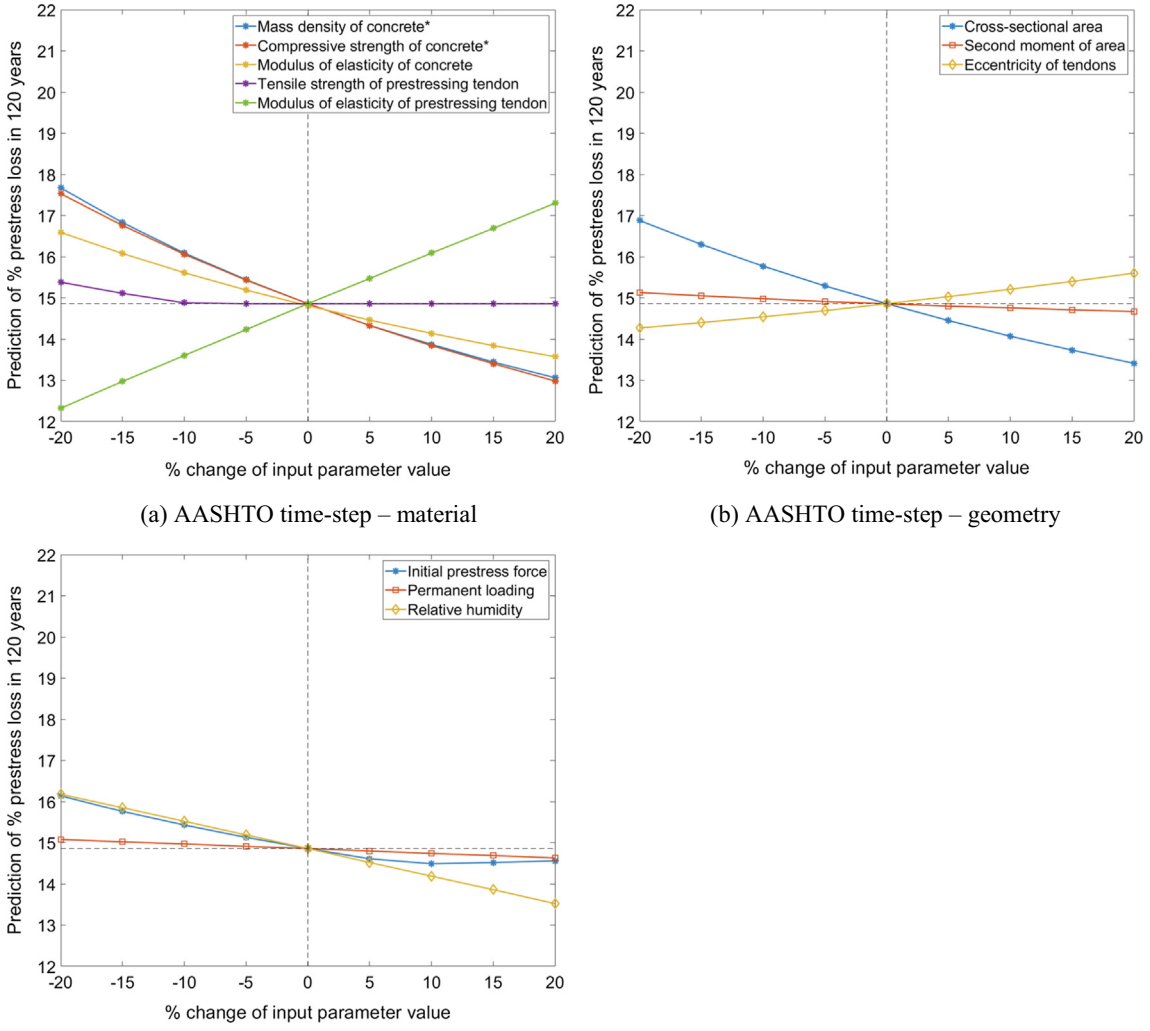

(a) AASHTO time-step – material (b) AASHTO time-step – geometry

(c) AASHTO time-step – loading and environment

Fig. 5. Sensitivity analysis results for AASHTO method.*Note: Change of concrete mass density would simultaneously change the estimations of concrete compressive strength and concrete modulus of elasticity in AASHTO-LRFD. Change of concrete compressive strength would simultaneously change the estimation of concrete mass density in AASHTO-LRFD.

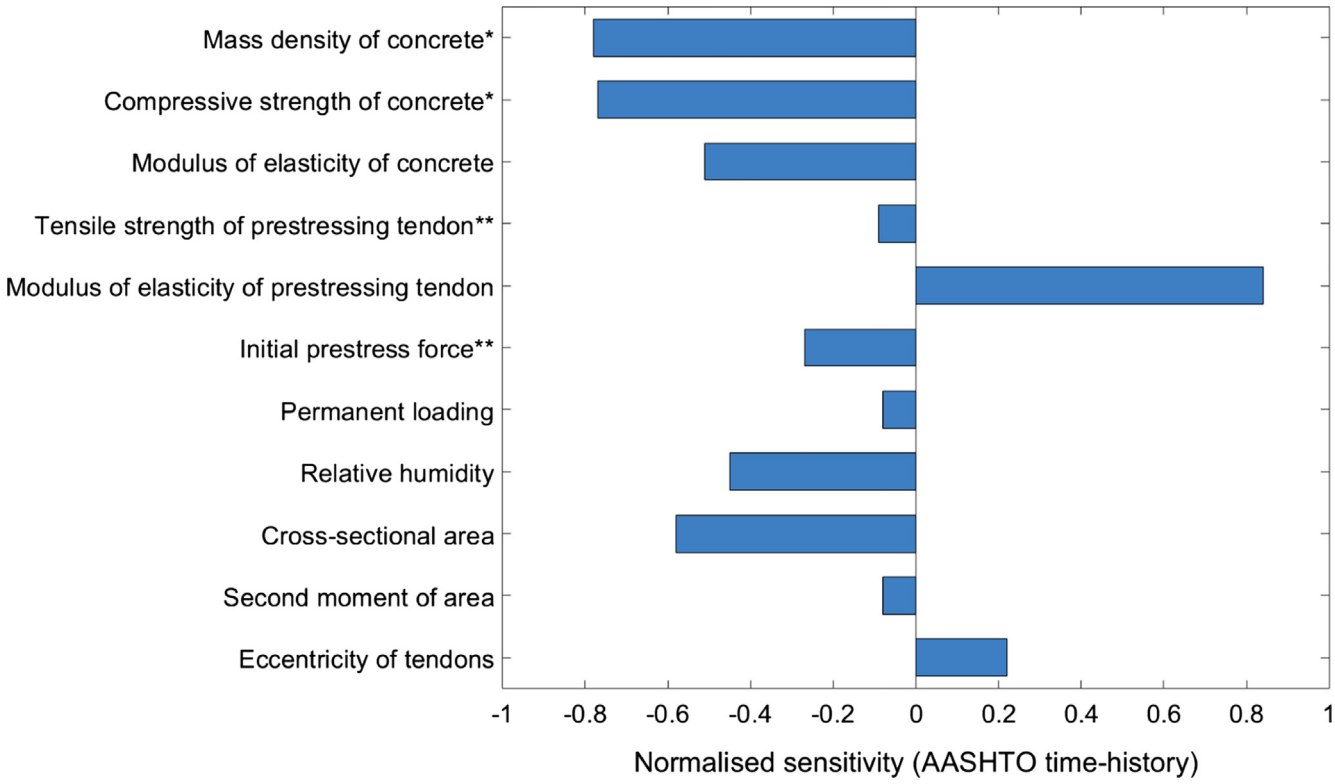

Fig. 6. Sensitivity analysis results for AASHTO method: normalised sensitivity.*Note: Change of concrete mass density would simultaneously change the estimations of concrete compressive strength and concrete modulus of elasticity in AASHTO-LRFD. Change of concrete compressive strength would simultaneously change the estimation of concrete mass density in AASHTO-LRFD.**Note: Relationship between input parameter and output prestress loss prediction is nonlinear.

iii. Geometry (cross-sectional area of concrete beam (uncracked cross-section), A_c, second moment of area (uncracked cross-section), I_c, and eccentricity of prestressing tendons (in uncracked cross-section), e_{cp}): Across all three methods, A_c has a large effect on prestress loss prediction, I_c has almost no effect and e_{cp} has a relatively small effect.
iv. Loading (initial prestress force, P_{jack}, and permanent loading (self-weight and quasi-permanent), $M_{sw} + M_{qp}$): In EC2, the relationship between P_{jack} and prestress loss prediction is highly nonlinear, which is due to the nonlinear relationship between relaxation loss prediction ΔP_{CR} and σ_{pi} ($=P_{jack}/A_c$ for time t = 0). In AASHTO-LRFD, the relationship between P_{jack} and prestress loss prediction is also nonlinear, which is due to the nonlinear relationship between relaxation loss ΔP_{pCR} and stress in prestressing strands immediately after transfer f_{pt} (which depends on the initial stress), as shown in Table 4. Across all three methods, permanent loading has a small effect on prestress loss prediction compared to other parameters.
v. Environmental conditions (relative humidity, RH): RH has a relatively large effect on the final prestress loss prediction, which is as expected given that variations in RH can have a considerable effect on both concrete shrinkage and creep.

In summary, the parameters which have significant effects on prestress loss predictions include concrete material properties, steel material properties, initial prestressing force, concrete beam cross-sectional area and relative humidity. Of these parameters, the values of concrete material properties, initial prestressing force and relative humidity are particularly uncertain, either because they are not directly measured (e.g. initial prestressing force and relative humidity) or because the measurements are highly variable (e.g. concrete material properties).

4. Monitoring results and discussion

4.1. Pre-installation behaviour of prestressed girders

The very early age behaviour of prestressed girders (i.e. prior to casting of in-situ concrete deck) was evaluated and discussed in a previous study by Butler et al. [27]. This previous study found that the measured prestress losses were slightly larger compared to the EC2 predictions but overall they have a reasonable agreement (on average around 2% difference in terms of the percentage prestress loss six months after beam casting). The measured prestress losses of TY7 and TYE7 beams during the first six months after casting were 79% and 72% of the EC2 predictions of ultimate prestress losses, respectively.

4.2. Effect of deck casting and curing

The first effect of deck casting is the additional dead load (i.e. self-weight of the cast in-situ concrete deck) applied to the concrete girders. As a result, M_{sw} would increase accordingly from 116 kNm to 267.6 kNm on 13 July 2015 (refer to Table 1). During curing and continued hydration of the concrete bridge deck slab, the girders and the deck were assumed to be perfectly bonded to form a composite section. Therefore, the new composite section geometry would be characterised by a new composite cross-sectional area, A_c, moment of area, I_c, and a revised prestressing strand eccentricity, e_{cp}. As a result of the formation of a new composite section geometry, there would be induced stress redistribution and differential creep, as described by Hendy and Smith [11].

In addition to differential creep, differential shrinkage would also occur. Due to the difference in age between the deck slab concrete and the girder concrete, the girder would have already experienced a significant amount of concrete shrinkage prior to the

time of deck casting and therefore would undergo shrinkage at a lower rate than the deck concrete. As the concrete deck would experience larger shrinkage strains compared to the concrete girder (i.e. creating differential shrinkage strains), a compressive force would be exerted along the top surface of the concrete girder, which would result in an additional loss of total prestress in the tendons.

4.3. Comparison of predicted and measured prestress losses

4.3.1. FOS strain measurements

Strain and temperature measurements were taken at ten uniformly spaced FBG sensors along one top and one bottom prestressing strands for each girder (i.e. 40 measurement points for each girder, 20 for strain and 20 for temperature). In addition, BOTDR continuous strain measurements were also taken along one top and one bottom prestressing strands for each girder, as shown in Fig. 2. The strain measurements are plotted in Figs. 7–10, which consider a baseline strain equal to those recorded just prior to detensioning. Overall, there is a reasonable agreement between the BOTDR strain values and the FBG strain values. The main discrepancies between FBG data and BOTDR data in this case study are: (i) The BOTDR data for the top of BM2 and BM3 (i.e. the top of two TY7 beams) shows much lower reduction in strain (i.e. lower prestress loss) for the first three months after beam casting compared with the corresponding FBG data (also shown in Butler et al. [27]), which is clearly anomalous; however, the subsequent measurements of strain reduction from the two sets of data have close agreement; (ii) The BOTDR data of BM1 and BM9 (TYE7 beams) shows larger reduction in strain at 9 months (and 9 months onwards) after beam casting compared with the corresponding FBG data; and (iii) For the bottom of BM1, the BOTDR measurements show 'strain recovery' from 9 months after casting, which makes little engineering sense and may be due to erroneous readings at 9 months after casting. A discrepancy between distributed and discrete FOS static strain measurements, with the same order of magnitude (100με), was reported in a previous study by Sigurdardottir and Glisic [28]. Brillouin Optical Time-Domain Analysis (BOTDA) was used in that case study for distributed strain measurements, which has a higher level of precision in measurement (±20με for temperature compensated strain, as specified in [28]) compared to BOTDR.

From the FBG dataset, similar behaviour can be observed for the same type of beam (i.e. comparing BM2 and BM3 – TY7 internal beams; and comparing BM1 and BM9 – TYE7 edge beams) and different behaviour across different beam types, which is less the case for the BOTDR dataset. Specifically, it can be seen from the FBG dataset that the prestress loss differences between 3 months after casting and pre-service baseline are much larger for TY7 internal beams than for TYE7 edge beams. This makes engineering sense as: (i) the internal beams are more loaded than the edge beams due to the loads of ballast, sleepers and rails above internal beams; and (ii) the edge beams have pre-cast deck above from Day 55 while the internal beams have a second stage beam casting on Day 55 prior to the in-situ deck casting, resulting in lower differential shrinkage and creep. Furthermore, across all four beams, the top of each beam shows a larger prestress loss from three months to nine months after beam casting compared with the bottom of

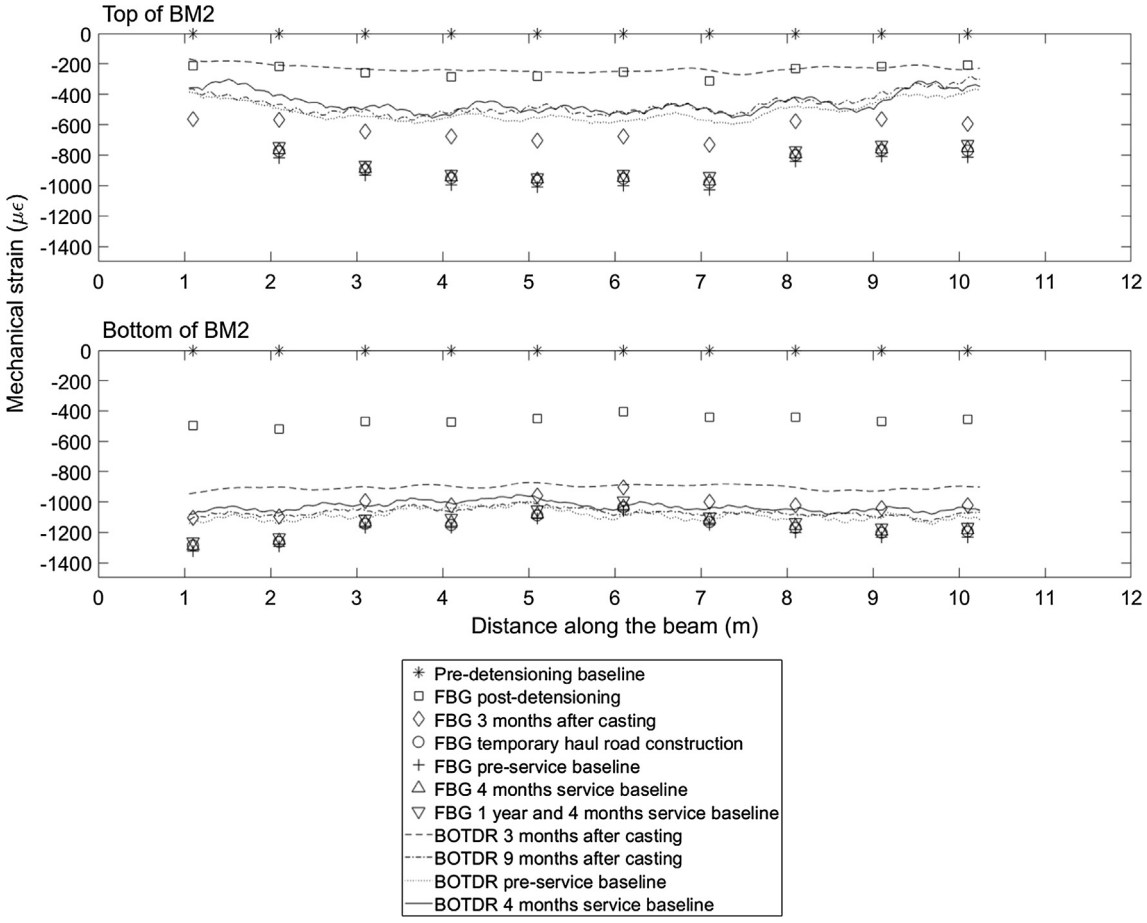

Fig. 7. Evolution of the distributed (BOTDR and FBG sensors) strain profile at the top and bottom of BM2 (baseline = pre-detensioning).

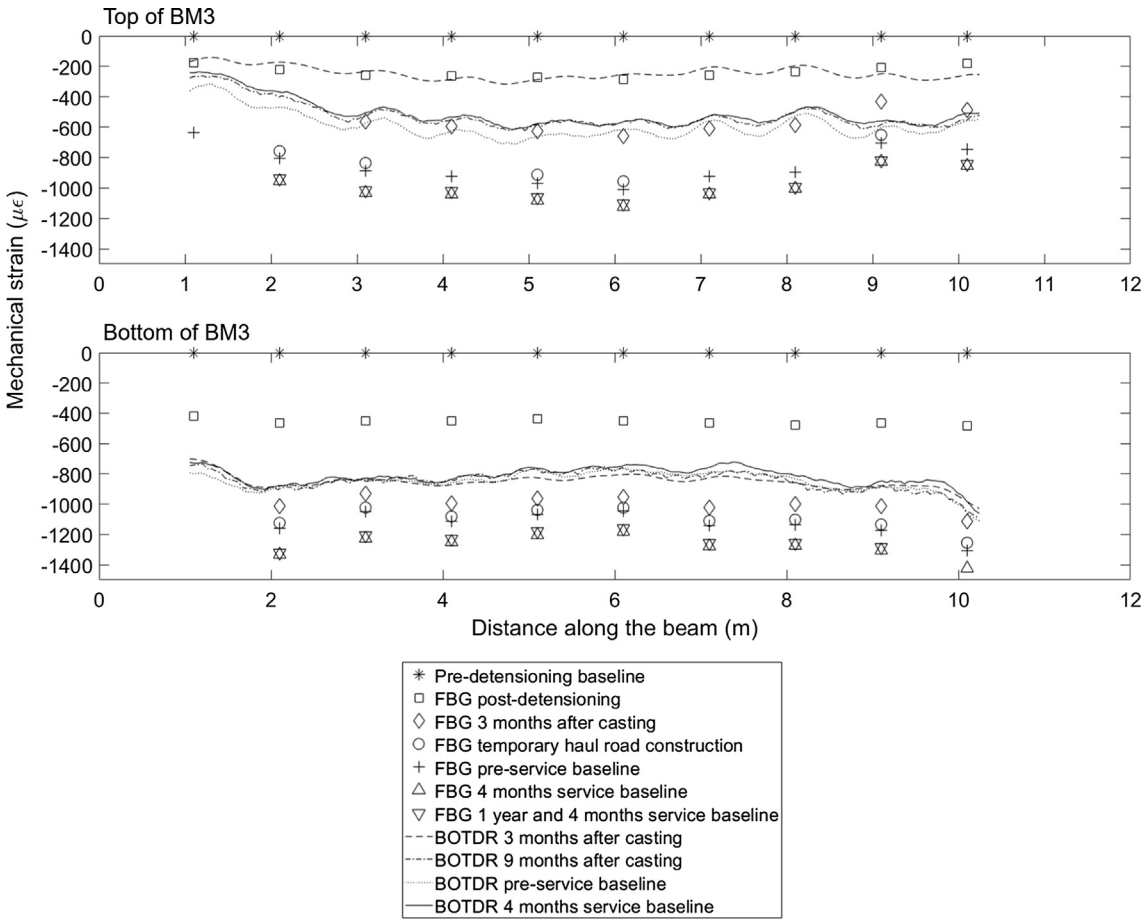

Fig. 8. Evolution of the distributed (BOTDR and FBG sensors) strain profile at the top and bottom BM3 (baseline = pre-detensioning).

the beam. This may be due to differential shrinkage as a result of the deck being cast six months after the beams, which would induce more compression at the top of each beam. In addition, this effect of larger prestress loss at the top is more significant for BM2 and BM3 (TY7 beams) than for BM1 and BM9 (TYE7 beams). This may be due to the fact that there was already a second stage beam casting for BM1 and BM9 on Day 55 prior to the deck casting and the strain measurements at three months after beam casting, and therefore the effect of differential shrinkage due to deck casting would be much smaller for BM1 and BM9. These observations add confidence to the accuracy of the FBG dataset for further processing and interpretation.

In summary, although the exact reasons behind the discrepancy between BOTDR and FBG measurements in this case study are uncertain, it is likely the result of a combination of effects:

i. The BOTDR data acquisition was affected by frequent errors with the analyser during the detensioning stage. This was likely due to the cold ambient temperatures at the time. In this case, temperature compensation for the BOTDR cables was performed using FBG temperature measurements. It is also possible that the BOTDR system was giving erroneous strain measurements at the detensioning stage, leading to higher uncertainty in BOTDR strain values. Therefore, the early-age BOTDR data for the top of BM2 and BM3, which is clearly anomalous, may be discarded for further processing and interpretation.
ii. Temperature compensation for BOTDR in particular may not be accurate due to inaccurate temperature coefficient values, which were assumed to be constant along the BOTDR cables. In addition, the BOTDR measurements have a lower level of precision (i.e. higher uncertainty in value) than the FBG measurements. Specifically, the FBGs can measure strain changes within ± 5με while the BOTDR can measure strain changes within ± 50με. The higher uncertainty in BOTDR temperature measurements compared with FBG temperature measurements results in higher uncertainty in the temperature compensation for the BOTDR cables and thus adds additional uncertainty to the temperature-compensated strain values.
iii. The BOTDR has a spatial resolution (i.e. averaging distance for strain measurements) of 50 cm. Therefore, concrete cracks and the associated localised strain concentrations would be measured by the BOTDR cables and be significantly reduced due to averaging effects. However, these same localised strain peaks originating at cracks may not be measured by the FBG sensors which are located at discrete points which may not correspond to the crack locations. In this case study, since no surface cracking was observed during the construction of the monitored beams, it may be assumed that the concrete remained uncracked and thus this averaging effect of BOTDR may not be significant for the discrepancies between FBG and BOTDR measurements.
iv. Other effects can also contribute to the discrepancy, such as the robustness of sensors to their installation environment, the variation in bonding conditions between the FOS sensors and the concrete surrounding the prestressing strands, the variation in FOS sensor attachment methods, and the variation in strain across the section (note that FBG and BOTDR sensors are attached to different prestressing strands).

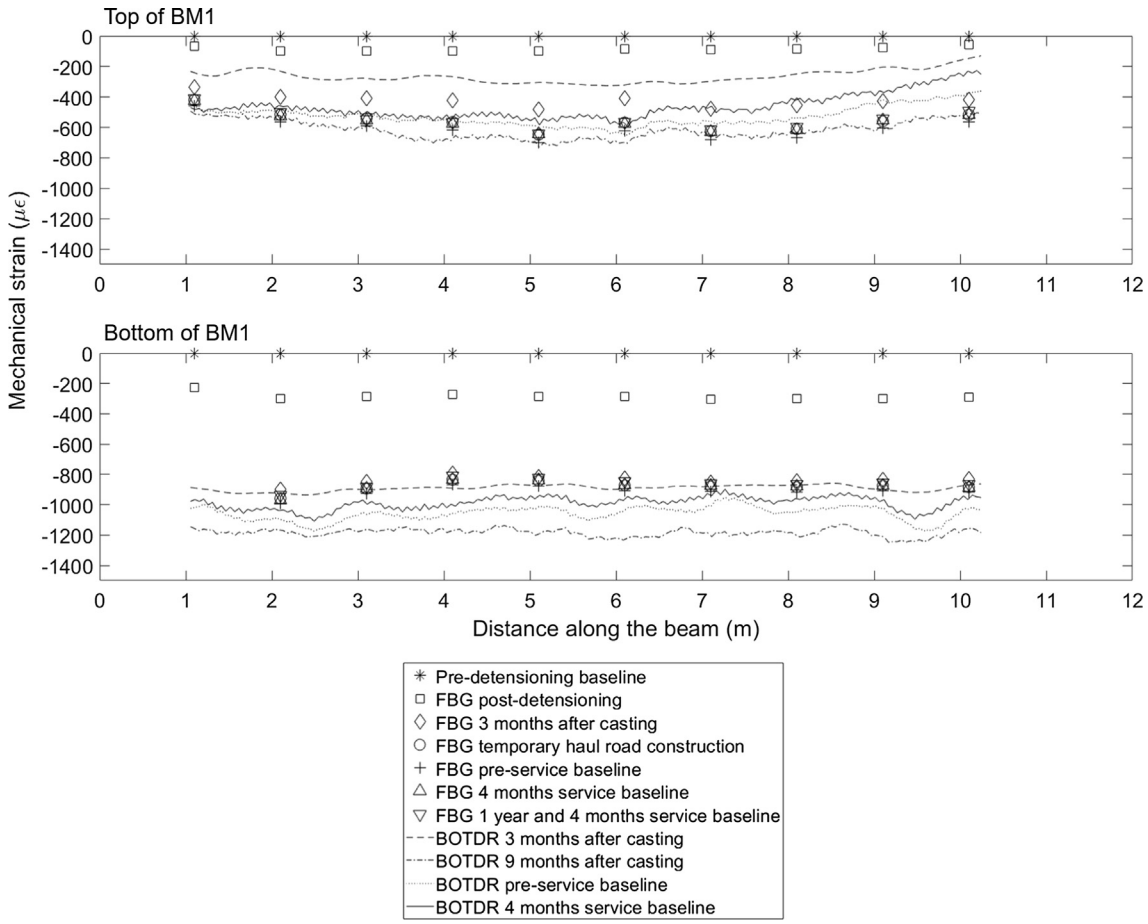

Fig. 9. Evolution of the distributed (BOTDR and FBG sensors) strain profile at the top and bottom of BM1 (baseline = pre-detensioning).

Fig. 11 shows the estimated strain changes at the centroidal level of each girder based on FBG measurements, with baseline set at pre-detensioning (i.e. 29 Jan 2015 for TY7 beams, BM2 and BM3, and 13 Jan 2015 for TYE7 beams, BM1 and BM9). These are based on the FBG strain readings near the midspan of each girder. In general, the TYE7 edge beams experienced lower prestress losses compared with the TY7 internal beams. There appears to be some consistent 'strain recovery' on the order of 50με from the last two sets of data (14 July 2016 and 7 July 2017, corresponding to 4 months in service and 1 year and 4 months in service, respectively) across BM1, BM2 and BM9. This 'strain recovery' is also observed from the BOTDR strain data (refer to Figs. 7–10). This may be due to the effects of seasonal change and in-service live loading on the physical response of the bridge such as support settlements. In a previous study by Abdel-Jaber and Glisic [24], the seasonal influence on strain response as a result of support settlements has also been found. The sudden drop of prestress level for BM3 at 4 months in service appears to be anomalous, either due to faulty sensor readings or some physical condition change of the girder. The majority of prestress losses were measured to have occurred during the first three months following de-tensioning.

4.3.2. Comparison of code predictions and sensor measurements

Based on the comparison between FBG and BOTDR strain results, prestress losses were calculated using the FBG strain results only as the BOTDR strain results have larger uncertainty in their values. It should be noted that the values of concrete properties (in particular, concrete strength) used in the calculations were estimated based on material testing rather than conservative code or specification values. The measured value from material testing was considered as a mean value rather than a characteristic value (i.e. 5th percentile). In addition, no partial safety factors for material or loading were applied. These assumptions were made to provide more realistic prestress loss behaviour to enable more meaningful comparisons between code predictions and sensor measurements. Fig. 12 presents the results of FBG measured, EC2 predicted and AASHTO predicted prestress losses, with a baseline set at pre-detensioning (i.e. prior to transfer of prestress).

The prestress loss predictions calculated using the time-step methods were lower compared to those predicted using the basic method. It appears that in this case study prestress loss predictions calculated using the EC2 simplified method, rather than the EC2 time-step method, have closer agreement with the measured prestress losses in terms of absolute magnitude. However, as shown from the sensitivity analysis, inaccurate input parameter values can have a noticeable influence on code predictions. While prestress loss predictions from the simplified method continue to grow at a relatively fast rate (based on the final prestress loss prediction (%), i.e. the total design life prestress loss)), both the measured prestress losses and the prestress loss predictions from the time-step methods begin to level off at an earlier point in time. The reason for the anomalous readings after 500 days (especially the sudden increase in prestress loss) for BM3 is not entirely known and may be due to measurement error or actual physical change of the beams. Overall, the code predictions of prestress losses slightly underestimated the prestress losses back-calculated from the sensor measurements.

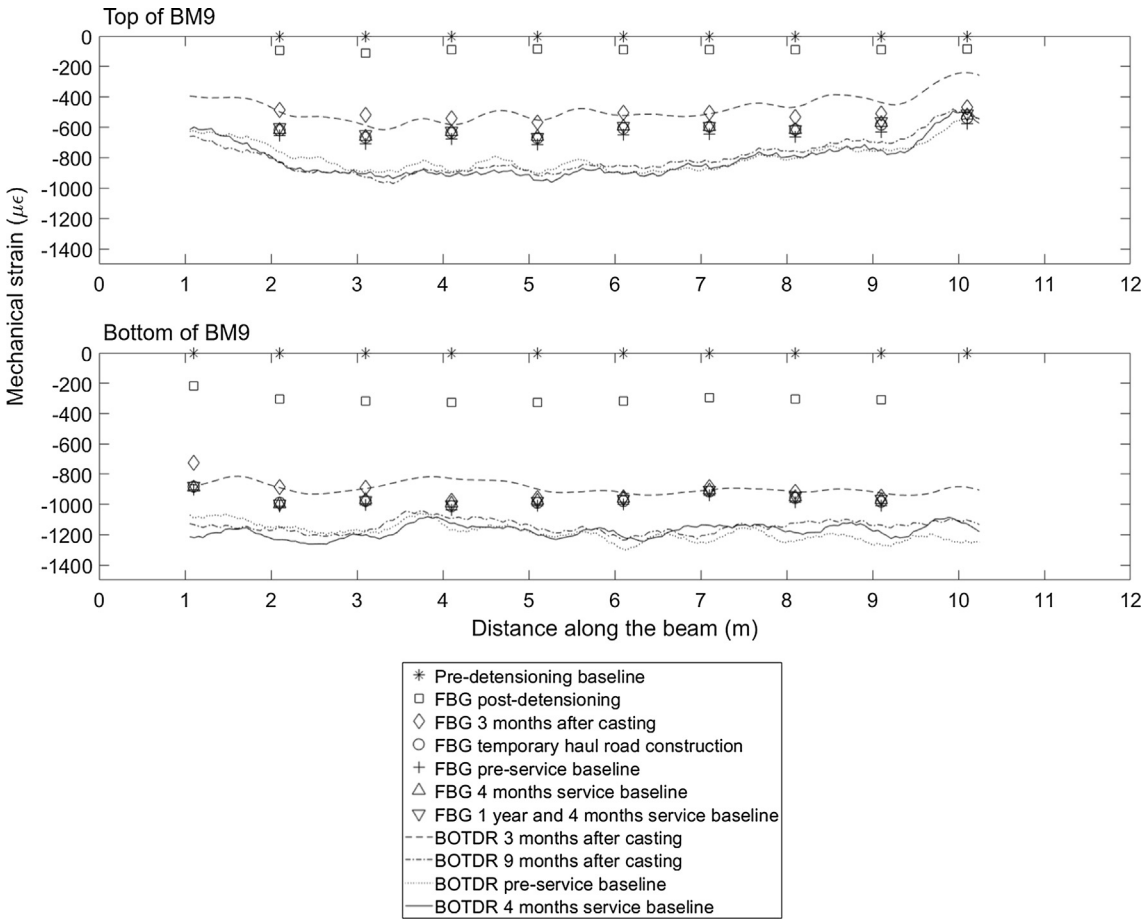

Fig. 10. Evolution of the distributed (BOTDR and FBG sensors) strain profile at the top and bottom of BM9 (baseline = pre-detensioning).

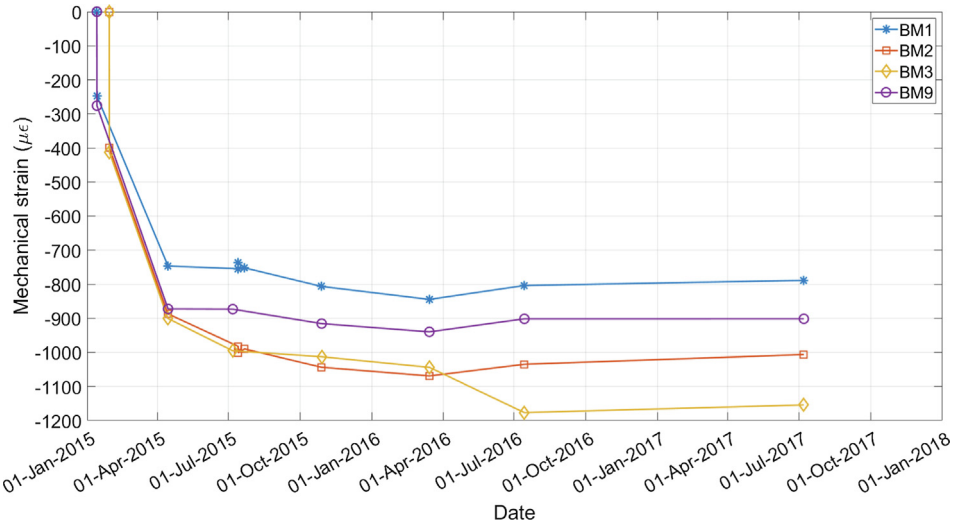

Fig. 11. Strain changes at centroidal level of the four beams (BM1, BM2, BM3 and BM9) over time, based on FBG measurements (baseline = pre-detensioning).

4.3.3. Effect of differential shrinkage

As mentioned previously, differential shrinkage resulting from segmental construction can cause additional prestress loss. The effect of differential shrinkage can be calculated using Eqs. (5) and (6), as described and discussed by Hendy and Smith [11],

$$\varepsilon_{diff} = \varepsilon_{sh,slab}(\infty) - \left(\varepsilon_{sh,beam}(\infty) - \varepsilon_{sh,beam}(t_1)\right) \quad (8)$$

$$F_{sh} = \varepsilon_{diff} E A_{slab} \frac{(1\text{-}e^{-\phi})}{\phi} \quad (9)$$

where

F_{sh} = Axial restrained force
ε_{diff} = differential shrinkage strain

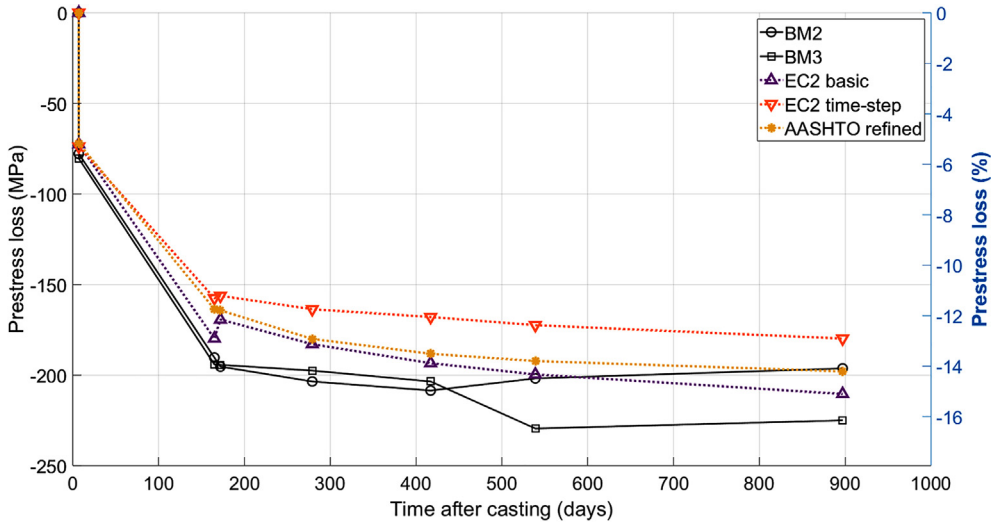

(a) TY7 beams

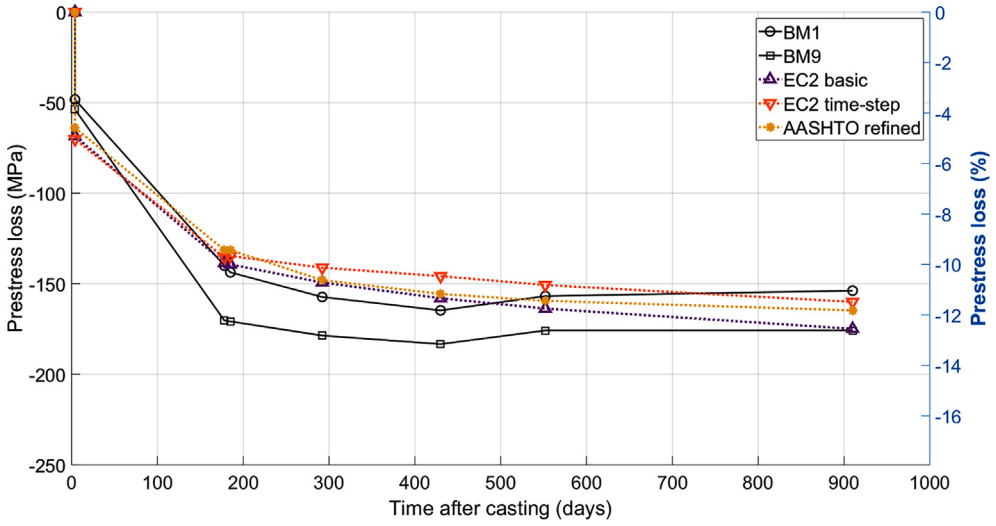

(b) TYE7 beams

Fig. 12. Evolution of measured prestress losses with time for the TY7 and TYE7 beams.

$\varepsilon_{sh,beam}(t_1)$ = shrinkage strain of the precast beam after casting the slab
$\varepsilon_{sh,beam}(\infty)$ = total shrinkage strain of the precast beam
$\varepsilon_{sh,slab}(\infty)$ = total shrinkage strain of the slab
ϕ = creep ratio

The predicted effect of differential shrinkage for the beams in this study is shown in Table 5. Note that unlike TY7 beams, TYE7 beams had a second stage beam casting on Day 55 after casting. The effect of differential shrinkage on prestress loss predictions for the TY7 and TYE7 girders were found to be negligible.

Table 5
Effect of differential shrinkage.

Additional prestress losses due to differential shrinkage (MPa and %)	EC2 method based on Hendy and Smith [11]	
	TY7 beams	TYE7 beams
1 year and 4 months in-service (Day 897 for TY7 beams and Day 910 for TYE7 beams, after beam casting)	2.9 (0.21%)	0.6 (0.04%)
120 years (Day 43,800 after beam casting)	5.4 (0.39%)	0.8 (0.06%)

4.4. Summary of key findings on field measurements and different predictive models

Based on the above findings, the code predictions of prestress losses, with no partial material or loading factors and using the mean values of material properties and loadings, slightly underestimate (generally by less than 1% prestress loss) but have a reasonable agreement with the FOS measured prestress losses. Based on the sensitivity analysis, this difference may be due to inaccurate estimations of various input parameters (e.g. material properties, initial prestress force, relative humidity, etc.) into the code equations. Both code predictions and FOS measurements show that the majority of prestress losses occurred within the first three months after beam casting. Furthermore, compared with the FOS measurements, the underestimation of code predictions is relatively more significant for early-age prestress losses and almost negligible two to three years after beam casting. This may be because code-based equations for prestress losses were derived

based on life cycles of more than 50 years and therefore they would yield poor early-age predictions.

It was also found that the time-step methods provided better predictions of prestress loss evolution over time. Specifically, while the prestress loss predictions from the simplified method continue to increase at a relatively faster rate over a long period of time (well beyond two years after beam casting), both the measured prestress losses and the prestress loss predictions using the time-step methods appear to level off within the first three years under normal conditions (i.e. no significant damage or deterioration). The predicted final loss from the simplified method is also higher than the predicted final losses from the time-step methods. Overall, the close agreement between code predictions and field measurements give some confidence to the accuracy of the predictive models in EC2 and AASHTO-LRFD for prestress losses, given that the real environmental and operational conditions are often difficult to predict and model.

5. Conclusions

This study has evaluated the prestress loss behaviour (over two and a half years) of four prestressed concrete beams installed on a railway bridge in Staffordshire, U.K. The beams were monitored during various stages of their construction (including beam installation, deck placement, etc.) and during their operation under in-service train loads (for approximately one year and four months). Prestress losses were successfully measured by an array of fibre optic sensors which were designed to be adequately robust for permanent installation and long-term operation. The installed sensors consisted of both distributed (BOTDR) and discrete (FBG) fibre optic sensors. The time-dependent prestress loss behaviour, which included the effects of steel relaxation, concrete shrinkage and concrete creep, was investigated in detail. Three methods were used to estimate long-term prestress losses: one simplified method (based on EC2) and two time-step methods (based on EC2 and AASHTO-LRFD). The time-step methods were able to account for the interrelationships between various prestress loss mechanisms and the remaining level of prestress in tendons over time. To evaluate the potential reasons for the differences between code predictions and FOS measurement, a comprehensive sensitivity analysis along with a qualitative uncertainty analysis were conducted to identify parameters of key importance to the final prestress loss prediction. The sensitivity analysis revealed that concrete material properties, steel material properties, initial prestress force, concrete beam cross-sectional area and relative humidity all have significant influence on final prestress loss predictions (in both MPa and %). It was found that code predictions slightly underestimate the FOS measurement of prestress loss (generally by less than 1%) but overall, there was a close agreement, particularly for medium- or long-term prestress losses (i.e. two years after beam casting). Both the prediction models and sensor measurement results indicated that most of the prestress losses occurred during the first three months following beam casting. Both the time-step method predictions and sensor measurements showed that the rate of prestress loss began to slow within the first three years under normal conditions (i.e. with no significant signs of damage or deterioration). Sensor measurements also revealed that the effect of differential shrinkage between the concrete beams and the cast-in-situ concrete deck slab on the change in prestress loss was negligible (i.e. less than 0.5%).

Based on the findings of this study, simplified methods appear to provide better estimates of the amount of early-age prestress loss while time-step methods appear to be better at estimating long-term losses. Future work will focus on developing systematic approaches for interpreting the discrepancy between real measurement and code predictions and investigating how field measurement can help reduce uncertainty in design and operation. The performance of post-tensioned structures will also be investigated using distributed and discrete FOS sensor technologies.

Overall, it is useful to monitor a bridge structure from the start of its lifecycle (i.e. construction and start of operation) to establish a performance baseline, i.e. 'normal' behaviour, for future structural health monitoring and bridge management. The subsequent sensor measurements can be used to validate design models and assumptions to improve the future design of similar projects.

CRediT authorship contribution statement

Cong Ye: Conceptualization, Methodology, Formal analysis, Writing - original draft. **Liam J. Butler:** Conceptualization, Data curation, Writing - review & editing. **Mohammed Z.E.B. Elshafie:** Supervision, Writing - review & editing. **Campbell R. Middleton:** Supervision, Writing - review & editing.

Declaration of Competing Interest

The authors declare that they have no known competing financial interests or personal relationships that could have appeared to influence the work reported in this paper.

Acknowledgement

The authors thank the EPSRC and Innovate UK for funding this research through the Cambridge Centre for Smart Infrastructure and Construction (CSIC) Innovation and Knowledge Centre (EPSRC grant reference number EP/L010917/1); the invaluable facilitation of the installation work from Liam Brunning of Explore Manufacturing and his team; the on-site assistance of Niamh Gibbons (formerly of CSIC), Jason Shardelow and Peter Knott of CSIC, Mahul Patel of CH2M HILL (formerly of CSIC), Hyungjoon Seo of Xi'an Jiaotong-Liverpool University (formerly of CSIC) and Jules Birks of Mott MacDonald (formerly of CSIC); the technical assistance in sensor deployment and procurement of Cedric Kechavarzi and Philip Keenan of CSIC; James Oliver, Matthew Timmis, Brad Stanaway and Phil Holland of Laing O'Rourke; Ruth Platt and Mike Henwood of Atkins for providing their invaluable support for this project; and the Laing O'Rourke Centre for Construction Engineering and Technology (University of Cambridge) for facilitating and supporting this research. Additional data related to this publication is available at the University of Cambridge data repository. https://doi.org/10.17863/CAM.49678.

References

[1] Network Rail "Bridge List", Online Available: https://www.networkrail.co.uk/ 2015 Accessed: 25-Jun-2019.
[2] S. Bourne, Prestressing: recovery of the lost art, Struct. Eng. 91 (2) (2013) 12–22.
[3] C.R. Middleton, P.R.A. Fidler, P.J. Vardanega, Bridge Monitoring: A Practical Guide, ICE Publishing, London, UK, 2016.
[4] G.T. Webb, P.J. Vardanega, P.R.A. Fidler, C.R. Middleton, Analysis of structural health monitoring data from Hammersmith Flyover, J. Bridg. Eng. 19 (6) (2014) 05014003, https://doi.org/10.1061/(ASCE)BE.1943-5592.0000587.
[5] F.C. Lea, C.R. Middleton, "Reliability of Visual Inspection of Highway Bridges", Technical Report, Cambridge University Engineering Department, 2002.
[6] M. Moore, B. Phares, B. Graybeal, D. Rolander, and G. Washer, "Reliability of Visual Inspection for Highway Bridges, Volume I: Final Report," Technical Report. Federal Highway Administration, 2001.
[7] CEN (European Committee for Standardization), EN 1992-1-1:2004 - Eurocode 2: Design of concrete structures - Part 1-1: General rules and rules for buildings. 2004.
[8] American Association of State Highway and Transportation Officials (AASHTO), AASHTO-LRFD Bridge Design Specifications, Second ed. Washington DC, 1998.
[9] International Federation for Structural Concrete (fib), CEB-FIP Model Code 90. London, UK: Thomas Telford Ltd., 1993.

[10] American Concrete Institute (ACI) Committee 209, Prediction of Creep, Shrinkage and Temperature Effects in Concrete Structures, vol. 92. Farmington Hills, MI, 1997.
[11] C.R. Hendy, D.A. Smith, Designers' Guide to EN 1992–2 - Eurocode 2: Design of concrete structures. Part 2: Concrete bridges, Thomas Telford Ltd., London, 2007.
[12] E. OBrien, A. Dixon, E. Sheils, Reinforced and Prestressed Concrete Design to EC2. The complete process, Second., Spon Press, Oxon, UK, 2012.
[13] A.E. Naaman, Pretressed Concrete Analysis and Design: Fundamentals, 2., Techno Press, Ann Arbor, MI, 2004.
[14] C. Middleton, P. Vardanega, G. Webb, P. Fidler, "Smart Infrastructure – Are we delivering on the promise?," in Keynote Paper: 6th Australian Small Bridges Conference, 2014, no. May, 2014.
[15] G.T. Webb, P.J. Vardanega, C.R. Middleton, Categories of SHM deployments: technologies and capabilities, J. Bridg. Eng. 20 (11) (2014) 04014118, https://doi.org/10.1061/(asce)be.1943-5592.0000735.
[16] P.J. Vardanega, G.T. Webb, P.R.A. Fidler, C.R. Middleton, J. Collins, Assessing the potential value of bridge monitoring systems, Proc. Inst. Civ. Eng. - Bridg. Eng. 170 (1) (2016) 87–88, https://doi.org/10.1680/jbren.16.00027.
[17] J.M.W. Brownjohn, P.-Q. Xia, H. Hao, Y. Xia, Civil structure condition assessment by FE model updating: methodology and case studies, Finite Elem. Anal. Des. 37 (10) (Sep. 2001) 761–775, https://doi.org/10.1016/S0168-874X(00)00071-8.
[18] W.E. Daniell, J.H.G. Macdonald, Improved finite element modelling of a cable-stayed bridge through systematic manual tuning, Eng. Struct. 29 (3) (2007) 358–371, https://doi.org/10.1016/J.ENGSTRUCT.2006.05.003.
[19] J. Jang, A. Smyth, Bayesian model updating of a full-scale finite element model with sensitivity-based clustering e2004, Struct. Control Heal. Monit. 24 (11) (2017), https://doi.org/10.1002/stc.2004.
[20] H. Schlune, M. Plos, K. Gylltoft, Improved bridge evaluation through finite element model updating using static and dynamic measurements, Eng. Struct. 31 (7) (2009) 1477–1485, https://doi.org/10.1016/J.ENGSTRUCT.2009.02.011.
[21] E.C. Bentz, N.A. Hoult, Bridge model updating using distributed sensor data, Proc. Inst. Civ. Eng. - Bridg. Eng. 170 (1) (2017) 74–86, https://doi.org/10.1680/jbren.15.00030.
[22] G.T. Webb, P.J. Vardanega, N.A. Hoult, P.R.A. Fidler, P.J. Bennett, C.R. Middleton, Analysis of fiber-optic strain-monitoring data from a prestressed concrete bridge, J. Bridg. Eng. 22 (5) (2017) 05017002, https://doi.org/10.1061/(asce)be.1943-5592.0000996.
[23] M.P. Collins, D. Mitchell, Prestressed concrete structures, Response Publications, Toronto, 1997.
[24] H. Abdel-Jaber, B. Glisic, Monitoring of long-term prestress losses in prestressed concrete structures using fiber optic sensors, Struct. Heal. Monit. 18 (1) (2019) 254–269, https://doi.org/10.1177/1475921717751870.
[25] H. Huang, S.-S. Huang, K. Pilakoutas, Modeling for assessment of long-term behavior of prestressed concrete box-girder bridges, J. Bridg. Eng. 23 (3) (2018) 04018002, https://doi.org/10.1061/(ASCE)BE.1943-5592.0001210.
[26] H. Sousa, J. Bento, J. Figueiras, Assessment and management of concrete bridges supported by monitoring data-based finite-element modeling, J. Bridg. Eng. 19 (6) (2014) 05014002, https://doi.org/10.1061/(ASCE)BE.1943-5592.0000604.
[27] L.J. Butler, N. Gibbons, P. He, C. Middleton, M.Z.E.B. Elshafie, Evaluating the early-age behaviour of full-scale prestressed concrete beams using distributed and discrete fibre optic sensors, Constr. Build. Mater. 126 (2016) 894–912, https://doi.org/10.1016/J.CONBUILDMAT.2016.09.086.
[28] D.H. Sigurdardottir, B. Glisic, On-site validation of fiber-optic methods for structural health monitoring: Streicker Bridge, J. Civ. Struct. Heal. Monit. 5 (4) (2015) 529–549, https://doi.org/10.1007/s13349-015-0123-x.